Quantifying the effect of baryon physics on weak lensing tomography

Elisabetta Semboloni[1⋆], Henk Hoekstra[1], Joop Schaye[1], Marcel P. van Daalen[1,2], Ian G. McCarthy[3]

[1]*Leiden Observatory, Leiden University, P.O. Box 9513, 2300 RA , Leiden, The Netherlands*
[2]*Max Planck Institute for Astrophysics, Karl-Schwarzschild Straße 1, 85741 Garching, Germany*
[3]*Kavli Institute for Cosmology, University of Cambridge, Madingley Road, Cambridge CB3 0HA, United Kingdom*

29 June 2012

ABSTRACT

We use matter power spectra from cosmological hydrodynamic simulations to quantify the effect of baryon physics on the weak gravitational lensing shear signal. The simulations consider a number of processes, such as radiative cooling, star formation, supernovae and feedback from active galactic nuclei (AGN). Van Daalen et al. (2011) used the same simulations to show that baryon physics, in particular the strong feedback that is required to solve the overcooling problem, modifies the matter power spectrum on scales relevant for cosmological weak lensing studies. As a result, the use of power spectra from dark matter simulations can lead to significant biases in the inferred cosmological parameters. We show that the typical biases are much larger than the precision with which future missions aim to constrain the dark energy equation of state, w_0. For instance, the simulation with AGN feedback, which reproduces X-ray and optical properties of groups of galaxies, gives rise to a $\sim 40\%$ bias in w_0. We also explore the effect of baryon physics on constraints on $\Omega_{\rm m}$, σ_8, the running of the spectral index, the mass of the neutrinos and models of warm dark matter. We demonstrate that the modification of the power spectrum is dominated by groups and clusters of galaxies, the effect of which can be modelled. We consider an approach based on the popular halo model and show that simple modifications can capture the main features of baryonic feedback. Despite its simplicity, we find that our model, when calibrated on the simulations, is able to reduce the bias in w_0 to a level comparable to the size of the statistical uncertainties for a Euclid-like mission. While observations of the gas and stellar fractions as a function of halo mass can be used to calibrate the model, hydrodynamic simulations will likely still be needed to extend the observed scaling relations down to halo masses of $10^{12}\,h^{-1}\,M_\odot$.

Key words: Gravitational lensing:weak, surveys - large-scale structure of the Universe - cosmological parameters - Cosmology: theory

1 INTRODUCTION

The discovery that the expansion of the Universe is accelerating is arguably one of the most significant discoveries of modern cosmology. We lack, however, a theoretical framework to explain the observations. For instance, current measurements can be explained by a cosmological constant or dynamic mechanisms (e.g., quintessence). The field driving the acceleration has been dubbed "dark energy", which can be parametrised by an equation-of-state w_0 (and additional evolving parameters). Modifications of the laws of gravity on cosmological scales have been considered as well (for a recent review, see for example Uzan 2007).

Observations of type Ia supernovae provided the first

evidence for the accelerated expansion (Perlmutter et al. 1999; Riess et al. 2007; Amanullah et al. 2010). Further support has come from observations of the cosmic microwave background (e.g., Komatsu et al. 2011), baryon acoustic oscillations (e.g., Eisenstein et al. 2005; Percival et al. 2010) and gas fractions of massive clusters (e.g., Allen et al. 2008). These methods allow us to constrain the properties of dark energy solely by studying the expansion history of the Universe and do not distinguish between modified theories of gravity that do not alter the expansion history.

Studies of the growth of structure are sensitive to both dark energy and modifications of gravity, and are therefore of great interest. The interpretation of the observations is complicated by the fact that most of the matter is in the form of dark matter. Fortunately, inhomogeneities of the matter distribution cause the light of background sources to be differentially deflected. This leads to co-

---

⋆ sembolon@strw.leidenuniv.nl

herent alignments in the shapes of these galaxies, which can be related directly to the power spectrum of matter density fluctuations. This phenomenon is referred to as "weak gravitational lensing" and when applied to the study of large-scale structure, it is also known as "cosmic shear".

The cosmic shear signal has been measured using large ground-based surveys (e.g., Hoekstra et al. 2006; Fu et al. 2008) and from space (e.g., Massey et al. 2007; Schrabback et al. 2010). As discussed by the Dark Energy Task Force (DETF; Albrecht et al. 2006), it is one of the most promising probes of dark energy. Space-based missions are currently planned with the aim to constrain the dark energy equation of state with a relative precision of $\sim 1\%$. The interpretation of the signal will, however, require exquisite knowledge of the power spectrum, well into the non-linear regime.

In order to exploit the statistical power of these future data sets, we need to be able to model the power spectrum with percent accuracy. To date, the interpretation of cosmic shear measurements rely on results based on N-body simulations that contain only collisionless (dark matter) particles. Under the assumption that the evolution of the large-scale structure is mainly described by the evolution of the dark matter distribution, this should lead to fairly accurate results. Recently, Heitmann at al. (2010) developed an 'emulator' which is able to provide dark matter only models with 1% accuracy on scales larger than a megaparsec.

However, a complete description of the matter fluctuations should also include baryon physics. Bernstein (2009) suggests to account for the effect of baryons on two-point weak lensing measurements by adding an unknown component to the power spectrum which is expressed using Legendre polynomials. The nuisance of the baryons is then included in the figure of merit (Albrecht et al. 2006) by marginalising over this component. Similarly, Kitching & Taylor (2010) propose a path-marginalisation technique and claim that this procedure reduces the figure of merit by 10%. In contrast, Zentner, Rudd & Hu (2008) suggest that constraining baryonic feedback and cosmology at the same time would degrade the figure of merit by about $30\% - 40\%$. From those studies it emerges that self-calibrating techniques are very promising although the strength of the result relies on prior assumptions; because of that it seems clear that the better we understand how various mechanisms affect the density distribution of the baryons, the better we can choose priors in the self-calibration procedures. For this reason it is important to study the effect of baryonic feedback directly using hydrodynamic simulations and this is the approach we adopt in this paper.

Hydrodynamic simulations are much more expensive than collisionless N-body simulations, and it has only recently become possible to simulate cosmological volumes with reasonable resolution. These simulations aim mainly to reproduce the properties of galaxies and the intergalactic medium, and to do that they need to account for processes such as radiative cooling, star formation, stellar mass loss, chemical enrichment and outflows driven by supernovae and AGN. To complicate the situation further, it is not yet clear which processes one needs to include in the simulations to mimic the observed Universe and the simulations still lack the resolution to model all relevant processes from first principles. The OverWhelmingly Large Simulations (OWLS) project (Schaye et al. 2010) represents an effort in that direction. The main goal of the OWLS project is to study how the properties of large-scale structures, galaxies and the intergalactic medium change in different scenarios, by producing a large number of simulations and by varying parameters independently. Comparisons with observations allow one to establish which mechanisms are required to

better describe our Universe. One of the main results of the OWLS project is that the simple insertion of baryons, star formation and feedback from supernovae, cannot reproduce the characteristics of groups of galaxies. Accounting for AGN feedback, however, results in good agreement with both X-ray and optical observations (McCarthy et al. 2010).

Importantly for cosmic shear studies, van Daalen et al. (2011) used the OWLS runs to show that the resulting power spectrum of matter fluctuations depends strongly on the adopted baryon physics out to surprisingly large scales. In particular, their model for AGN feedback leads to significant changes compared to scenarios with only star formation and relatively inefficient feedback from supernovae. In this latter scenario, cooling baryons change the profiles of the haloes, generating more compact cores and increasing power on small scales (e.g., Jing et al. 2006; Rudd et al. 2008, Guillet et al. 2010; Casarini et al. 2011). To prevent the formation of overly luminous galaxies and to reproduce the X-ray properties of groups, extremely efficient feedback is required. AGN feedback can prevent the overcooling of the baryonic component by ejecting large quantities of gas at high redshift, when the supermassive black holes were growing rapidly (McCarthy et al. 2010; 2011). Consequently, AGN feedback can modify the power spectrum in a dramatic way, decreasing the scale below which cooling increases the power, and significantly reducing the power up to very large scales. Levine & Gnedin (2006) used a simple toy model to manually include AGN outflows in collisionless simulations and to show that AGN can potentially drastically change the power spectrum, although they were unable to predict the sign and the magnitude of the effect. More recently, van Daalen et al. (2011) predicted, using a fully hydrodynamic simulation that reproduces optical and X-ray observations of groups of galaxies, a $\sim 10\%$ decrease in total power relative to a dark matter only simulation on scales of $0.1 - 10 \ h^{-1} \ \mathrm{Mpc}$ at $z = 0$.

Ignoring the effects of baryon physics may therefore lead to biases in the constraints of cosmological parameters inferred from cosmic shear studies. In this paper we use the power spectra tabulated by van Daalen et al. (2011) to evaluate the effects of a number of feedback scenarios. In addition, we provide a simple, yet rather effective approach to reduce the bias of cosmological parameters. We show that this kind of approach will be crucial for upcoming surveys because the bias will be much larger than the statistical uncertainties, if left uncorrected.

This paper is organised as follows. In section 2 we describe the set of simulations we use for this work. In section 3 we examine how cosmic shear statistics are affected. In section 4 we quantify the biases introduced when ignoring the effects of baryon physics. In section 5 we show that it is possible to recover realistic power spectra and to remove (most of) the biases by making use of simple models that are calibrated to match the star and gas fractions of the simulated groups. Cosmic shear cannot only constrain the properties of the dark energy, but can also be used to study the running of the spectral index, warm dark matter and massive neutrinos. In section 6 we evaluate the consequences of baryonic feedback on the ability of cosmic shear to constrain those effects. Finally, we conclude in section 7.

2   SIMULATIONS

To examine the physics that drives the formation of galaxies and the evolution of the intergalactic medium, the OverWhelmingly Large Simulations (OWLS) project includes over 50 large, cosmological,

hydrodynamic simulations run with a modified version of the SPH code Gadget (last described in Springel 2005). A range of physical processes was considered, as well as a range of model parameters. In this paper we use a subset of OWLS for which we will give a brief description, inviting the reader to find more details in the papers where the simulations are presented. Note that all simulations have been performed with the same initial conditions[1]. The simulations considered here are (following the naming convention of Schaye et al. 2010):

• DMONLY: a dark matter only simulation, of the kind commonly used to compute the non-linear power spectrum which is needed in weak lensing studies. It is therefore the reference to which we compare the other simulations.

• REF: although it is not the reference simulation for the study presented here, this simulation includes most of the mechanisms which are thought to be important for the star formation history (see Schaye et al. 2010 for a detailed discussion) but not AGN feedback. The implementation of radiative cooling, star formation, supernovae driven winds, and stellar evolution and mass loss have been described in Wiersma, Schaye & Smith (2009), Schaye & Dalla Vecchia (2008), Dalla Vecchia & Schaye (2008), and Wiersma et al. (2009), respectively. This simulation represents a standard scenario assumed in cosmological hydrodynamic simulations.

• DBLIMFV1618: this simulation has been produced using the same mechanisms as REF. The only difference between the two simulations is that in this simulation the stellar initial mass function (IMF) was modified to produce more massive stars when the pressure of the gas is high, i.e. in starburst galaxies and close to galactic centres. This is obtained by switching from the Chabrier (2003) IMF assumed in the REF model to a Baugh et al. (2005) IMF in those regions. There are both observational and and theoretical arguments to support a top-heavy IMF in those extreme conditions (e.g. Padoan et al. 1997; Baugh et al. 2005; Klessen et al. 2007; Maness et al. 2007; Dabringhausen et al. 2009; Bartko et al. 2010; Weidner et al. 2010). The IMF change causes the number of supernovae and the effect of stellar winds to increase resulting in a suppression of the SFR at smaller redshifts. However, this mechanism alone is not able to reproduce the observed SFR (see Schaye et al. 2010).

• AGN: a hydrodynamic simulation which differs from REF only by the inclusion of AGN. The AGN feedback has been modelled following Booth & Schaye (2009). In this approach AGN transfer energy to the neighbouring gas, heating it up and driving supersonic outflows which are able to displace a large quantity of baryons far from the AGN itself. Among the three simulations considered here, it is arguably the most realistic, as it is able to reproduce the gas density, temperature, entropy, and metallicity profiles inferred from X-ray observations, as well as the stellar masses, star formation rates, and stellar age distributions inferred from optical observations of low-redshift groups of galaxies (McCarthy et al. 2010).

To forecast the cosmic shear signal for the four different scenarios, we make use of the results of van Daalen et al. (2011), who tabulated the power spectra of matter fluctuations $P(k, z)$ in redshift slices over the redshift range $0 \leqslant z \leqslant 6$ for a number of OWLS runs. A detailed discussion of the procedure to compute the
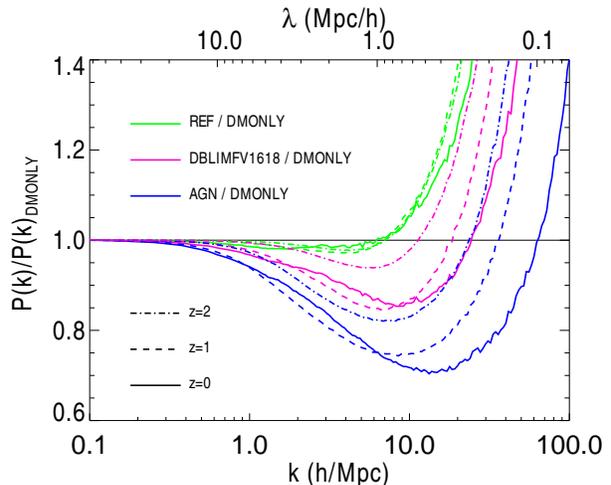
Figure 1. Ratio between the power spectrum of matter fluctuations measured from the simulations with baryons and the one measured from the DMONLY simulation. The ratio for the REF simulation is shown in green, the one for the AGN simulation is shown in blue, and the one for the DBLIMFV1618 model is shown in pink. Since the simulations have been carried out using the same initial conditions, deviations of the ratio from unity are due to the differences in baryon physics.

power spectrum and its accuracy can be found in van Daalen et al. (2011). Their convergence tests and noise estimations suggest that the power spectra estimated from OWLS are reliable up to at least $k \approx 10\,h\,\mathrm{Mpc}^{-1}$ over the range of redshifts we are interested in (i.e. $z \lesssim 1$, as the lensing signal is most sensitive to structures that are halfway between the observer and the source). At small k, the estimate of the power spectrum is affected by the finite size of the simulation box ($100\,h^{-1}\,\mathrm{Mpc}$ on a side). This is not a concern, because on these scales baryonic effects are very small and density fluctuations are in the linear regime, so that we can compute the power spectrum from theory instead.

Figure 1 shows the power spectrum measured for each simulation in three redshift bins normalised by the power spectrum of the dark matter simulation (DMONLY) at the same redshift. In the REF scenario (green), the presence of the baryons slightly suppresses the power spectrum at intermediate scales, due to the pressure of the gas. At smaller scales where baryons cool, the power spectrum is enhanced as the baryons fall into the potential wells. For this model, only the small scales are affected in an almost redshift independent way. The effect of baryon physics is more pronounced for the DBLIMFV1618 model, and depends on redshift. The AGN model leads to the largest difference compared to the DMONLY simulation. The amplitude of the power spectrum is strongly reduced on scales of $\sim 1 - 10\,h^{-1}\,\mathrm{Mpc}$ and the effect increases as the redshift decreases; this is in agreement with the results by McCarthy et al. (2011) who showed that because AGN remove low-entropy gas at early stages ($2 \lesssim z \lesssim 4$), the high-entropy gas left in the haloes does not cool down and form stars and the suppression of power becomes more and more accentuated at small scales.

The latter two scenarios are qualitatively similar, although the mechanisms are different: in the DBLIMFV1618 simulation baryons are removed due to the enhanced supernova feedback, whereas in the AGN scenario they are removed mostly by AGN feedback, at least for the more massive and thus strongly clustered haloes. Thus, the fraction of baryons which is removed is different,
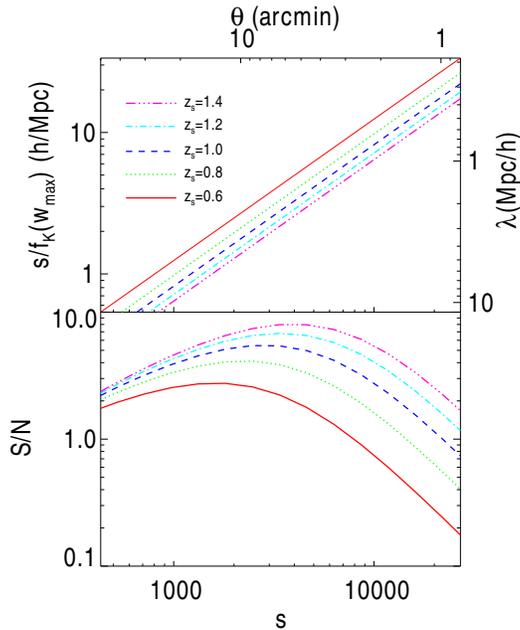
Figure 2. Top panel: relation between the wave number $k = s/f_K(w_{\mathrm{max}})$ and angular wave number s for various source redshifts. This relation shows, for a given source redshift, which k contributes most to the convergence power spectrum at a given s. For both s and k we show the corresponding real-space conjugate variables. Bottom panel: typical $P_\kappa(s)$ signal-to-noise ratio as a function of the wave number s. We show results for the same set of source redshifts as were shown in the upper panel.

as is the rate at which they are removed. At very small scales cooling still enhances structure formation, but the physical scale below which this occurs is smaller than in the REF simulation.

Although we will focus on a set of simulations which have been produced using the WMAP3 cosmology, van Daalen et al. (2011) compared a dark matter only simulation and an AGN simulation realised with the best-fit WMAP7 cosmology (Komatsu et al. 2011) and found that the difference is the same as between the AGN and DMONLY simulations used here. This implies that the relative effect of baryonic feedback does not change significantly with the cosmology, and thus that our conclusions are not restricted to a specific set of cosmological parameters.

3   EFFECT OF BARYONS ON TWO-POINT SHEAR STATISTICS

In this section we briefly introduce the basics of weak gravitational lensing by large-scale structure and how baryon physics affects the interpretation of the measurements. For a more extensive review of cosmic shear, see for example Hoekstra & Jain (2008) and Munshi et al. (2008). A thorough discussion of the theory of weak lensing and its applications is given in Bartelmann & Schneider (2001).

Massive structures along the line of sight deflect photons emitted by distant galaxies. Provided the source is small, the effect is a remapping of the source's surface brightness distribution: the source is both (de)magnified and sheared. In the weak lensing regime, the convergence κ gives the magnification (increase in size) of an image and the shear $\boldsymbol{\gamma}$ gives the ellipticity induced on an initially circular image. Under the assumption that galaxies are randomly oriented in the absence of lensing, the strength of

the tidal gravitational field can be inferred from the measured ellipticities of an ensemble of sources. The resulting complex shear $\boldsymbol{\gamma} \equiv \gamma_1 + i\gamma_2$ is a spin-2 pseudo vector, which can also be written as $\boldsymbol{\gamma} = \gamma \exp(2i\alpha)$, where α is the position angle of the shear.

If redshift information is available for the sources, one can compute the two-point shear correlation functions for galaxies in the ith and j^{th} redshift bins, which are defined as

$$\xi_+^{i,j}(\theta) = \langle \gamma_{i,\mathrm{t}}(\boldsymbol{\theta}_1)\gamma_{j,\mathrm{t}}(\boldsymbol{\theta}_2) + \gamma_{i,\times}(\boldsymbol{\theta}_1)\gamma_{j,\times}(\boldsymbol{\theta}_2) \rangle \quad (1)$$

$$\xi_-^{i,j}(\theta) = \langle \gamma_{i,\mathrm{t}}(\boldsymbol{\theta}_1)\gamma_{j,\mathrm{t}}(\boldsymbol{\theta}_2) - \gamma_{i,\times}(\boldsymbol{\theta}_1)\gamma_{j,\times}(\boldsymbol{\theta}_2) \rangle \quad (2)$$

where $\theta = |\boldsymbol{\theta}_1 - \boldsymbol{\theta}_2|$ and we have defined the tangential and cross components of the shear as: $\gamma_{\mathrm{t}} = -\mathcal{R}e(\gamma \exp(-2i\phi))$ and $\gamma_\times = -\mathcal{I}m(\gamma \exp(-2i\phi))$, with ϕ the polar angle of the separation vector $\boldsymbol{\theta}$. Note that the ensemble average depends only on the angular distance between the galaxies. The measurement of the redshift dependence of the cosmic shear signal greatly improves the constraints on cosmological parameters from weak lensing and is a key goal of current and future surveys. It is often referred to as weak lensing tomography (e.g. Hu 1999; Hu 2002), because it allows us to study the matter distribution in "slices". The correlation functions can be measured from a catalogue of galaxy shapes and they are related to the convergence cross-power spectrum:

$$\xi_{+/-}^{ij}(\theta) = \frac{1}{2\pi}\int_0^\infty \mathrm{d}s' s' \mathrm{J}_{0/4}(s'\theta)P_\kappa^{ij}(s'), \quad (3)$$

where J_0, J_4 are the 0th and the 4th order Bessel functions of the first 8kind. The convergence power spectrum $P_\kappa^{ij}(s)$ is related to the power spectrum of matter fluctuations $P(k, w)$ through (Kaiser 1998; Schneider et al. 1998):

$$P_\kappa^{ij}(s) = \frac{9H_0^4}{4c^4}\Omega_{\mathrm{m}}^2 \int_0^{w_{\mathrm{H}}} \mathrm{d}w \frac{g_i(w)g_j(w)}{a^2(w)}P\left(\frac{s}{f_{\mathrm{K}}(w)}, w\right), \quad (4)$$

with

$$g_i(w) = \int_w^{w_{\mathrm{H}}} \mathrm{d}w' p_i(w')\frac{f_{\mathrm{K}}(w' - w)}{f_{\mathrm{K}}(w')}, \quad (5)$$

where $f_{\mathrm{K}}(w)$ is the comoving angular distance, w is the radial comoving coordinate, w_{H} is the radial comoving coordinate of the horizon; H_0, Ω_{m} and $a(w)$ are the Hubble constant, the matter density parameter and the scale factor, respectively. The projected power spectrum depends on $p_i(w)$, the radial distribution of the sources in the ith redshift bin. Since s is the Fourier-conjugate of the angle θ, we can relate an angular scale to it through $s = 2\pi/\theta$.

Various two-point shear statistics that have been employed in the literature simply correspond to different filters of $P_\kappa(s)$ in Eqn. 4. Therefore, the detailed effect of baryonic feedback will depend somewhat on the statistic that is used, but this does not significantly affect our conclusions which are derived using $P_\kappa(s)$. Note that in the case of a full sky survey one could determine the $C(l)$ from a decomposition in spherical harmonics. For small angular separations $s \approx l$ and $l(l + 1)C(l) \approx s^2 P_\kappa(s)$.

3.1   Relevant scales

Cosmic shear results are typically presented in terms of angular scales, rather than the physical scales shown in Fig. 1. We therefore start by examining which angular scales are affected by baryon physics. To do so, we consider sources at a single redshift. In this
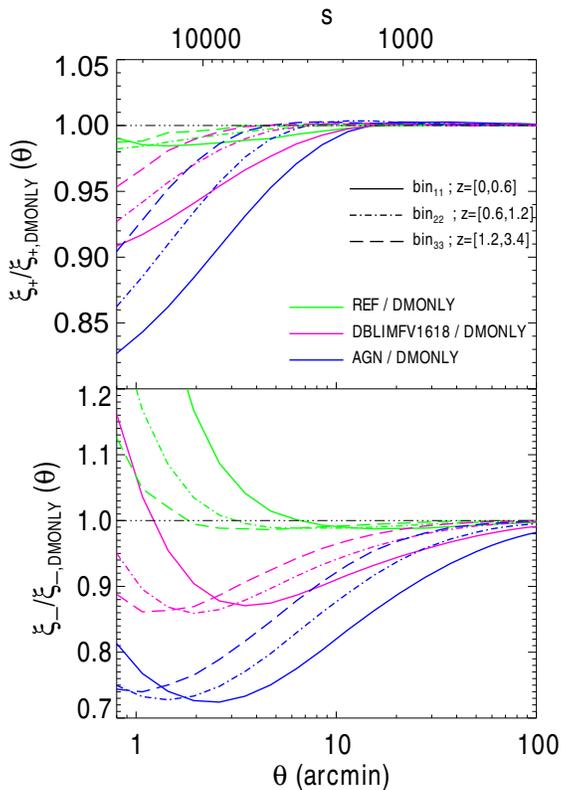
Figure 3. Top panel: ratio of the correlation function $\xi_+(\theta)$ for REF/DMONLY (green), DBLIMFV1618/DMONLY (pink) and AGN/DMONLY (blue) . The notation bin_{ij} indicates the correlation of sources from redshift bin i with sources from redshift bin j. Here, we show only results from the bins with $i = j$. Bottom panel: same as the upper panel but for the correlation function $\xi_-(\theta)$.

case one can show that the value of $P_\kappa(s)$ depends mostly on the density fluctuations with comoving wave numbers $\approx s/f_K(w_{\mathrm{max}})$ with $f_K(w_{\mathrm{max}})$ maximising the ratio $\frac{f_K(w_s-w)f_K(w)}{f_K(w_s)}$. In the top panel of Figure 2, we show, for various source redshifts z_s, the relation between the angular wave number s and the wave number $s/f_K(w_{\mathrm{max}})$ using the adopted WMAP3 cosmology. It shows, for example, that measuring the power spectrum $P_\kappa(s)$ at $s \sim 1 \times 10^4$ of galaxies with redshifts ~ 0.8, probes density fluctuations at scales $k \sim 10h\,\mathrm{Mpc}^{-1}$, where baryon physics is important.

However, one might wonder if the signal at arcminute scales is statistically important. To examine this, the bottom panel of Figure 2 shows a typical signal-to-noise ratio of $P_\kappa(s)$. The signal has been computed assuming a WMAP3 cosmology. The noise accounts for sampling and statistical noise, assuming a WMAP3 cosmology and a survey area $A = 20000\ \mathrm{deg}^2$, a number density of galaxies of $n = 30\ \mathrm{gal/arcmin}^2$ all placed at the same redshift z_s and with intrinsic ellipticity dispersion $\sigma_e = 0.33$ (see section 4 for more details on the noise computation). As one can see, the signal-to-noise ratio peaks at scales between 2 and 10 arcmin, where baryon physics is important.

Having established that cosmic shear studies are sensitive to

the scales where baryon physics modifies the power spectrum, we now want to quantify how various scenarios change the two-point shear statistics. For that we adopt a source redshift distribution that is representative of the CFHTLS-Wide (Benjamin et al. 2007) and a fair approximation for Euclid (Laurejis et al. 2009). We adopt the following parametrisation:

$$p(z) = \frac{\alpha}{(z + z_0)^\beta}\ , \qquad (6)$$

with $\alpha = 0.836$, $\beta = 3.425$, and $z_0 = 1.171$. We divide the source galaxies in three tomographic bins with limits [0, 0.6, 1.2, 3.4], which yields six cross-power spectra.

The top panel of Figure 3 shows the value of $\xi_+(\theta)$ measured for the various feedback scenarios, normalised by the results for DMONLY. The effect of baryons is small and limited to very small scales for the REF scenario. However, for DBLIMFV1618, and in particular for the AGN model, the difference with the DMONLY result is large and increases when the redshift of the sources decreases. The redshift dependence is the result of two effects. The first is a geometric one: when the redshift of the sources decreases, the physical scales probed by the lensing signal become smaller (see Figure 2). The second reason is the suppression of the amplitude of the power spectrum due to feedback, which becomes larger at late times (see Figure 1). The bottom panel of Figure 3 shows the value of $\xi_-(\theta)$ measured for the various feedback scenarios, normalised by the results for DMONLY. Notice that the bias for ξ_- is more pronounced out to larger scales. This is because ξ_- is much more sensitive to small-scale structures (i.e. to the shape of the power spectrum $P_\kappa(s)$ for large s).

3.2 Effect on cosmological parameter estimation

It is clear from Figure 1 that the change in the power spectrum is large in the case of the AGN and DBLIMFV1618 scenarios. The modification is, however, scale-dependent, which may help to ameliorate the problem, since this cannot be reproduced by varying cosmological parameters which predominantly affect the overall amplitude of the weak lensing power spectrum. In other words, it might be possible to separate the effects of baryonic feedback, or at least to identify them: the inferred values for cosmological parameters from weak lensing statistics are scale-dependent for the AGN and DBLIMFV1618 scenarios.

We first investigate the effect on the recovered value of σ_8, the rms fluctuation of matter in spheres of size $8\,h^{-1}$ Mpc. A complication to our analysis is the limited accuracy of the prescriptions for the non-linear power spectrum, be it Peacock & Dodds (1996) or the halofit approach (Smith et al. 2003) used here. We therefore cannot predict $\xi_{+,\mathrm{DMONLY}}(\theta, z_s)$ directly, but the procedure outlined below is accurate as the predictions should have the correct scaling as a function of σ_8. For the various feedback models we first define the ratio

$$R_{+,\mathrm{hydro}}(\theta, z_s) = \frac{\xi_{+,\mathrm{hydro}}(\theta, z_s)}{\xi_{+,\mathrm{DMONLY}}(\theta, z_s)}, \qquad (7)$$

as a function of source redshift z_s and angular scale θ. Here $\xi_{+,\mathrm{hydro}}(\theta, z_s)$ is the correlation function measured for REF, DBLIMFV1618 or AGN, whereas $\xi_{+,\mathrm{DMONLY}}(\theta, z_s)$ is the DMONLY correlation function. We use the halofit prescription (Smith et al. 2003) to compute $\xi_{+,\mathrm{halofit}}(\theta, z_s; \sigma_8)$, keeping all
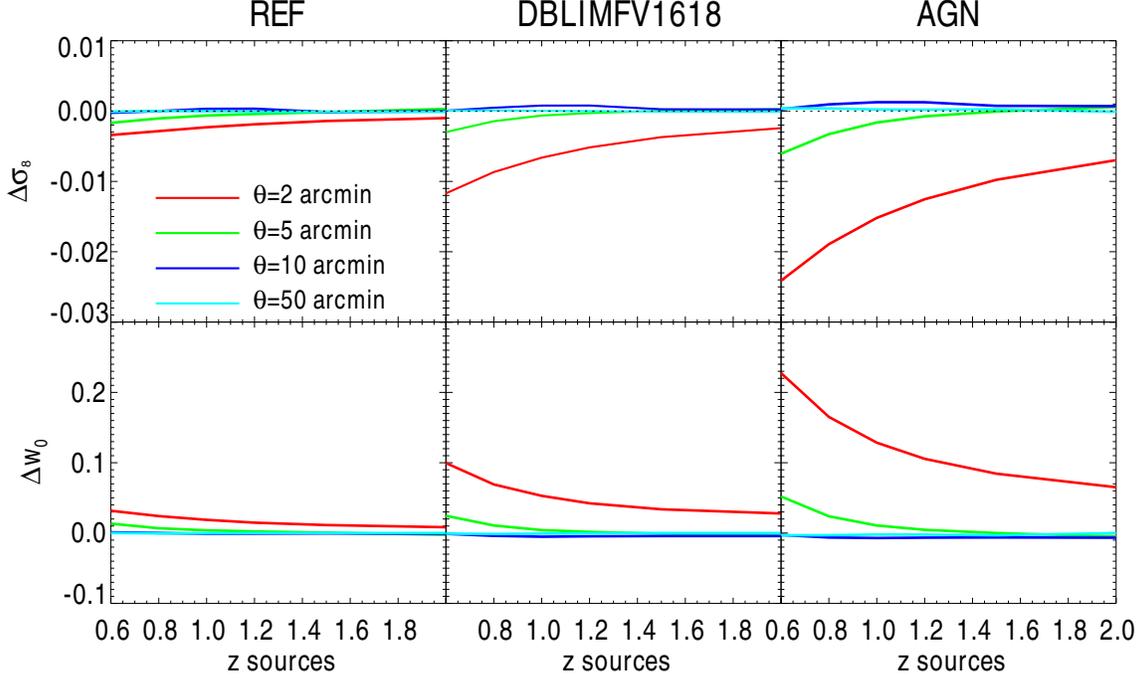
Figure 4. Top (bottom) panels show the deviation of the inferred σ_8 (w_0) from the true reference value $\sigma_{8,\mathrm{ref}} = 0.74$ ($w_{0,\mathrm{ref}} = -1$) as a function of source redshift, when the amplitude of the ellipticity correlation function $\xi_+(\theta)$ is used to estimate the cosmological parameter of interest (while the other parameters are kept at their reference values) and when we use halofit models (see text for details). The deviation depends on the angular scales that is used and is smaller for larger scales. The left panels show the results for the REF scenario, the middle panels for the DBLIMFV1618 and the right panels for the AGN scenario, which results in the largest biases.

other cosmological parameters fixed to the reference values. We define the ratio

$$R_{+,\mathrm{halofit}}(\theta, z_s; \sigma_8) = \frac{\xi_{+,\mathrm{halofit}}(\theta, z_s; \sigma_8)}{\xi_{+,\mathrm{ref,halofit}}(\theta, z_s)}, \qquad (8)$$

where $\xi_{+,\mathrm{ref,halofit}}$ is the halofit prediction for the reference cosmology. For each z_s and θ we find the value of σ_8 for which $R_{+,\mathrm{halofit}}(\theta, z_s) = R_{+,\mathrm{hydro}}(\theta, z_s)$. Hence, we compute by how much the value of σ_8 needs to change from the reference value if one ignores feedback processes and instead interprets the measurement of $\xi_+(\theta, z_s)$ in a dark matter only framework.

The top panels of Figure 4 show the resulting value $\Delta\sigma_8 = \sigma_8 - \sigma_{8,\mathrm{ref}}$ for which $R_{\mathrm{halofit}} = R_{\mathrm{hydro}}$ as a function of z_s for various values of θ. As we anticipated, the inferred values of σ_8 depend on angular scale, but the effect of baryon physics is modest, particularly for the REF simulation. For the AGN and DBLIMFV1618 models the effect is qualitatively the same and it is still only a few percent.

In models with a constant dark energy equation of state $P = w_0\rho$, the change of w_0 mainly leads to a change in the amplitude of the weak lensing power spectrum. It is therefore interesting to repeat the same analysis for models with dark energy. Note that if we vary the value of w_0, both the expansion history and the history of structure formation change. Because we normalise the amplitude of the fluctuations at the present time, decreasing the value of w_0 results in fluctuations that are larger at earlier times. On the other hand, a very negative equation of state increases the expansion rate.

Thus, the overall amplitude of the two-point shear statistics at a given scale and redshift depends on which of the two competing effects is dominant.

The bottom panels of Figure 4 show the values $\Delta w_0 = w_0 - w_{0,\mathrm{ref}}$ as function of the angular scale and source redshift. Compared to the bias in σ_8, the change in the inferred value of w_0 is more dramatic, reaching 20% for the AGN scenario, 10% for the DBLIMFV1618 scenario, and even for the REF scenario w_0 is few percent too high. Note that we did not consider a redshift dependent equation of state $w(z)$; also in that case we expect the estimated value of w to change as a function of the angular scale, leading to similar conclusions. These findings suggest that baryon feedback can lead to significant biases in cosmological parameters in the case of future cosmic shear studies. In the next section we will quantify this in more detail.

4 EFFECT ON LIKELIHOOD RESULTS

In this section we quantify the bias in the inferred values for w_0 and σ_8 if one interprets weak lensing measurements using dark matter derived models. To do so, we perform a likelihood analysis, where we define the posterior probability distribution as:

$$P(\mathbf{p}|\mathbf{d}) \propto P(\mathbf{p})\mathcal{L}(\mathbf{d}|\mathbf{p}) \qquad (9)$$

where $\mathbf{p}$ and $\mathbf{d}$ are vectors of parameters and observed data, respectively, and the likelihood $\mathcal{L}(\mathbf{d}|\mathbf{p})$ is given by:
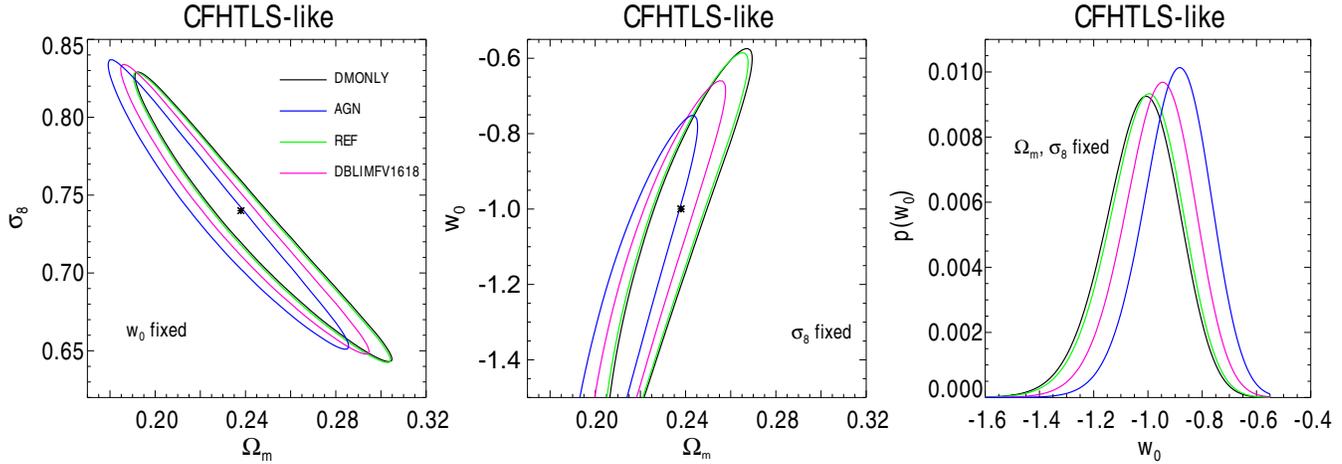
Figure 5. Left panel: $\Omega_\mathrm{m} - \sigma_8$ likelihood contours for a CFHTLS-like survey. Middle panel: $\Omega_\mathrm{m} - w_0$ likelihood contours for a CFHTLS-like survey. Right panel: posterior probability distribution for $p(w_0)$ obtained for $\sigma_8 = 0.74$ and $\Omega_\mathrm{m} = 0.238$. Solid contours mark the 68% confidence regions. The shifts relative to the DMONLY case indicate the presence of bias due to baryonic effects. The biases are largest for the AGN scenario.
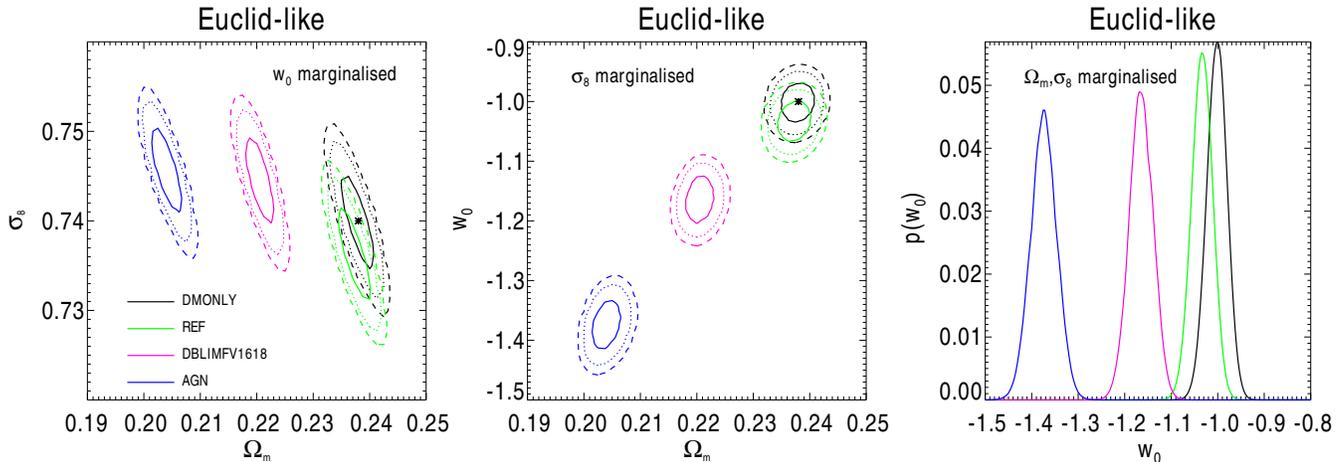

Figure 6. Left panel: joint constraints on $\sigma_8 - \Omega_\mathrm{m}$ for a Euclid-like survey. Solid, dotted and dashed lines mark the 68%, 95% and 99% confidence regions respectively. Middle panel: joint constraints on $\Omega_\mathrm{m} - w_0$. Right panel: posterior probability distribution for $p(w_0)$ marginalised over σ_8 and Ω_m. The shifts relative to the DMONLY case indicate the presence of bias due to baryonic effects. The biases are largest for the AGN scenario. Note that for the right panel the sign of the shift differs from what was found in Figure 5, because we now marginalise over the other parameters, rather than keeping them fixed.

$$\mathcal{L}(\mathbf{d}|\mathbf{p}) \propto \exp\left[-1/2(\mathbf{m}(\mathbf{p}) - \mathbf{d})\mathcal{C}^{-1}(\mathbf{m}(\mathbf{p}) - \mathbf{d})^T\right]. \quad (10)$$

Here $\mathbf{m}(\mathbf{p})$ is a model and $\mathcal{C}$ is the covariance matrix. We chose the data vector $\mathbf{d}$ to be $P_\kappa(s)$ sampled at twenty scales between $s = 10$ and $s = 6000$ for the six cross spectra introduced in section 3. The total data vector thus contains 120 measurements. We compute cosmological models $P_\kappa(s)$ at the same scales using the halofit prescription for the non-linear power spectrum. All the models use the transfer function by Eisenstein & Hu (1998) which accounts for the effect that baryons have on the power spectrum during the radiation-dominated epoch. In this way the linear power spectrum of our models is similar (Eisenstein & Hu is just an approximation) to the one used to establish the initial conditions of the OWLS simulations.

Throughout the paper we use flat priors $\Omega_\mathrm{m} = [0.160, 0.316]$ and $\sigma_8 = [0.65, 0.83]$, corresponding to the $\pm 3\sigma$ error-bars for WMAP7. We also adopt a flat prior of $w_0 = [-2.00, -0.6]$. We emphasise that uninformative priors are needed to study the bias, because (unbiased) information from external data may force the recovered values towards their unbiased values.

Following Takada & Jain (2004), we compute the covariance matrix in the Gaussian approximation. Note that the Gaussian approximation breaks down at small scales. This is because the non-linear evolution of the density field causes the modes to mix, resulting in non-zero off-diagonal terms. As a consequence, the value of the variance is increased (Semboloni et al. 2007; Takada & Jain 2009; Pielorz et al. 2010). Since we do not want to overestimate the impact of baryon physics by underestimating the error bars at small scales, we only consider modes $s \leqslant 6000$, which correspond to angular scales larger than $\theta \approx 3.5\mathrm{arcmin}$.

As before, we do not use the data vector $\mathbf{d}_\mathrm{hydro}$, which is measured from the simulations. Instead we construct a new data vector

$\mathbf{d}_{\rm fit}$:

$$\mathbf{d}_{\rm fit} = \frac{\mathbf{d}_{\rm halofit}}{\mathbf{d}_{\rm DMONLY}} \times \mathbf{d}_{\rm hydro}, \qquad (11)$$

where $\mathbf{d}_{\rm hydro}$ corresponds to $P_\kappa(s)$ from the REF, AGN, or DBLIMFV1618 simulation, and where $\mathbf{d}_{\rm DMONLY}$ is computed using the DMONLY simulation. The halofit approach is used to calculate $\mathbf{d}_{\rm halofit}$, which quantifies the dependence on the cosmology. If the halofit model described the power spectrum of the DMONLY simulation perfectly then the ratio in Eq. 11 would be unity for any component of the data vector and $\mathbf{d}_{\rm fit}$ would be merely $\mathbf{d}_{\rm hydro}$. This is, however, not the case because the halofit model has limited accuracy; moreover the set of simulations we use is relatively small so the measured power spectrum is affected by sampling variance. We are only interested in the comparison between dark matter only simulations and simulations with baryonic feedback. By using Equation 11 we can compute the bias in cosmological parameters that one would obtain by neglecting the existence of baryons, while minimising the limitations of the halofit prescription and sampling variance due to the finite size of the simulations.

We first consider a survey with area $A = 200 \deg^2$, galaxy number density $n = 15 \, \rm gal/arcmin^2$ and intrinsic ellipticity dispersion of galaxies $\sigma_e = 0.44$, which roughly corresponds to the CFHTLS-Wide survey (e.g., Hoekstra et al. 2006; Fu et al. 2008). The joint constraints on $\Omega_{\rm m}$ and σ_8 are presented in the left panel of Figure 5, whereas the constraints on $\Omega_{\rm m}$ and w_0 are displayed in the middle panel. Note that we keep the other parameter(s) fixed, rather than marginalising over them, because the statistical power of the CFHTLS is too limited to constrain them. The shifts in the likelihoods, compared to the DMONLY contours, indicate that the cosmological parameters are biased if a dark matter power spectrum is used to interpret the data. In agreement with our earlier findings, the shifts are small for the REF model and larger for the other two scenarios.

Based on the results of the previous section, we are most concerned about a bias in w_0. The right panel of Figure 5 shows the posterior probability for w_0, when the other parameters are kept fixed at their fiducial values. This result suggests that a dark matter only modelling of the CFHTLS signal will likely predict a value of w_0 which is about 10% less negative than the real one. However, the DMONLY peak lies at the edge of the 68% confidence region of the AGN scenario, thus the bias is similar to the statistical uncertainty. Note that since the CFHTLS-Wide has limited statistical power due to its modest survey area, we fixed the values of σ_8 and $\Omega_{\rm m}$ to constrain w_0, which affects the bias. We will see below that the bias is different (and increases) if we use a flat prior.

To reach a precision of a few percent, much larger projects are being planned. Of these, we focus on the space-based Euclid mission (Refregier et al. 2010), which aims to survey an area $A = 20000 \deg^2$ with a number density of galaxies of $n = 30 \, \rm gal/arcmin^2$ and intrinsic ellipticity dispersion $\sigma_e = 0.33$. This leads to much smaller statistical errors on the cosmological parameters. As shown in Figure 6, in this case the effect of baryons leads to significantly biased results. The left panel shows the constraints on $\Omega_{\rm m}$ and σ_8, while marginalising over the value of w_0. The likelihood contours for both the AGN and DBLIMFV1618 models are shifted towards lower values for $\Omega_{\rm m}$, and an only slightly higher σ_8. The consequences for the constraints on w_0 are even more dramatic, as is clear from the middle panel of Fig. 6. The bias in w_0 reaches almost 40% for the AGN scenario, as is also evident from the marginalised probability distribution shown in the right panel. The large bias is the consequence of the large modification of the
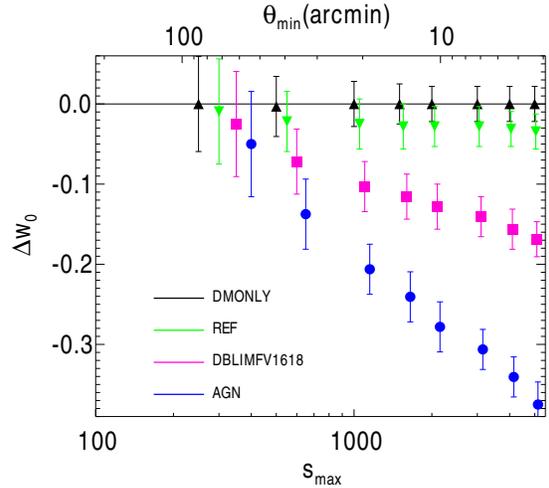

Figure 7. Difference Δw_0 between the best fit value of w_0 and the true reference value $w_0 = -1$ as a function of the maximum angular wavenumber $s_{\rm max}$ (or minimum scale $\theta_{\rm min}$) that is included in the likelihood analysis. The error bars represent the resulting 1σ uncertainties on w_0. Avoiding high wave numbers allows one to reduce the bias affecting the cosmological parameters at the cost of an increase of the statistical errors.

power spectrum at intermediate scales. Note that the shift in the value of w_0 in the right panel is in the direction opposite to what was found in Figure 4, because here we marginalised over the other parameters whereas they were kept fixed in Figures 4 and 5.

Since the bias arises due to differences in the power spectrum at relatively small angular scales θ, or large s, it is interesting to examine whether the bias can be reduced by leaving the large wave numbers out of the likelihood analysis. Figure 7 shows the maximum likelihood value of w_0 as a function of the maximum angular wave number $s_{\rm max}$, while marginalising over $\Omega_{\rm m}$ and σ_8. The error bars on the points indicate the 68% confidence regions. The bias is no longer statistically significant if the posterior probability for w_0 peaks well within one sigma from the reference value $w_0 = -1$. For the AGN model this is only achieved when $s < 500$ (this corresponds to a real space separation of more than 40 arcminutes!). However, drastically limiting the range of scales increases the statistical uncertainty by almost a factor of three. We therefore conclude that this approach is not viable and that one needs to account for the effects of baryon physics when computing the constraints on cosmological parameters.

5   REDUCING THE BIAS USING A SIMPLE MODEL

The results presented in the previous section suggest that one cannot ignore the effects of baryon physics on the matter power spectrum in the case of future lensing surveys. A complication is that the bias itself depends strongly on the details of the feedback model, but that we do not know for sure which of the feedback scenarios (and parameters) is correct. However, baryon physics also has an impact on other observables, which can be used to discriminate between models.

For example, McCarthy et al. (2010) showed that the AGN and REF simulations yield haloes with significantly different gas fractions. Similarly, the amount of gas that cools to form stars is different, leading to different luminosities. For both observables, the AGN simulation provided a good match to observations of groups

of galaxies whereas the REF simulation did not. In principle, such observations can be used to select hydrodynamic simulations that best describe our Universe. In this section, we will explore a different approach and show that those same observables can be used to modify the dark matter power spectrum such that it accounts for most of the effects of baryon physics.

5.1 Halo model

To predict the matter power spectrum analytically, we take advantage of the fact that the clustering of haloes of a given mass is known in the linear regime and that the average density profiles of dark matter haloes are specified by their mass. As shown by Seljak (2000), this "halo model" approach can reproduce the power spectrum into the non-linear regime, although some parameters have to be calibrated using numerical simulations.

The power spectrum is computed as the sum of two terms. The first one describes the correlation of the density fluctuations within the same halo. This Poisson term $P^{\mathrm{P}}(k)$ dominates on small scales and is given by

$$P^{\mathrm{P}}(k) = \frac{1}{(2\pi)^3} \int \mathrm{d}\nu f(\nu) \frac{M(\nu)}{\bar{\rho}} y[k, M(\nu)]^2, \quad (12)$$

where $\bar{\rho}$ is the mean matter density and $y[k, M(\nu)]$ is the Fourier transform of the density profile of a halo with virial mass $M(\nu)$ normalised such that:

$$y[k, M] = \frac{\int_0^{r_{\mathrm{vir}}} 4\pi r^2 \mathrm{d}r \frac{\sin(kr)}{kr} \rho(r)}{\int_0^{r_{\mathrm{vir}}} 4\pi r^2 \mathrm{d}r \rho(r)}, \quad (13)$$

where $\rho(r)$ is the density profile of the halo and r_{vir} its virial radius. The peak height ν of such an overdensity is defined as

$$\nu = \left[\frac{\delta_{\mathrm{c}}(z)}{\sigma(M)} \right]^2, \quad (14)$$

where δ_{c} is the linear theory value of a spherical overdensity which collapses at a redshift z. $\sigma(M)$ is the rms fluctuation in spheres that contain mass M at an initial time, extrapolated to z using linear theory. We use (Sheth & Tormen 1999):

$$\nu f(\nu) = A(1 + \nu'^{-p})\nu'^{1/2} \exp(-\nu'/2), \quad (15)$$

where $\nu' = a\nu$ with $a = 0.707$ and $p = 0.3$. The normalisation constant A is determined by imposing $\int f(\nu)\mathrm{d}\nu = 1$. Note that the function $f(\nu)$ is related to the halo mass function $\mathrm{d}n/\mathrm{d}M$ through

$$\frac{\mathrm{d}n}{\mathrm{d}M}\mathrm{d}M = \frac{\bar{\rho}}{M} f(\nu)\mathrm{d}\nu. \quad (16)$$

The second term, $P^{\mathrm{hh}}(k)$, describes the clustering of haloes and dominates on large scales. It is given by

$$P^{\mathrm{hh}}(k) = P_{\mathrm{lin}}(k)\left(\int \mathrm{d}\nu f(\nu)b(\nu)y[k, M(\nu)] \right)^2, \quad (17)$$

where $P_{\mathrm{lin}}(k)$ is the linear power spectrum, and the halo bias $b(\nu)$ is given by (Mandelbaum et al. 2005):

$$b(\nu) = 1 + \frac{\nu' - 1}{\delta_c} + \frac{2p}{\delta_c(1 + \nu'^p)}, \quad (18)$$

with $a = 0.73$ and $p = 0.15$. Finally, one generally assumes that the density profile is of the form (Navarro et al. 1995):

$$\rho(r) \propto \frac{1}{r(r + r_s)^2}, \quad (19)$$

where r_s is the scale radius. Numerical cold dark matter simulations have shown that this NFW profile is a fair description of the radial matter distribution for haloes with a wide range in mass. They also indicate that r_s is not a free parameter, but that it is related to the virial mass (albeit with considerable scatter). It is customary to account for this correlation by specifying a relation, between the concentration $c = r_{\mathrm{vir}}/r_s$ and the virial mass. We use the mass-concentration relation derived by Duffy et al. (2008). The virial mass and radius are related through $M_{\mathrm{vir}} = (4\pi/3)r_{\mathrm{vir}}^3\rho_c\delta_{\mathrm{vir}}$, where we use the fitting formula of Bryan & Norman (1998) to compute $\delta_{\mathrm{vir}}(z)$.

It is typically assumed that the total matter density can be described by the NFW profile. However, if the stars and the gas do not follow the dark matter profile, then the resulting mass profile and thus the power spectrum will be different. In the remainder of this section we will explore whether it is possible to simply modify the density profile to better describe the distribution of the baryons, and whether this model can reduce the biases discussed in the previous section. Because of the back-reaction of the baryons on the dark matter, baryonic effects will also induce changes in the dark matter distribution within haloes (e.g., Duffy et al. 2010) and in the dark matter power spectrum (van Daalen et al. 2011). For simplicity, we will, however, ignore this complication.

5.2 An improved halo model

The halo model is only a good description of the total matter distribution if the baryons trace the underlying dark matter distribution.

As feedback processes redistribute the baryons (which make up $\sim 17\%$ of the total amount of matter), we expect the total matter power spectrum to be modified. In this section we explore whether it is possible to predict the power spectrum from hydrodynamic simulations using 'observations' of the gas fraction and stellar mass (or luminosity).

Somogyi & Smith (2009) showed that in order to construct accurate models that include CDM and baryons one should treat the density field as a two-component fluid. The procedure that we use here, which is to compute the linear matter power spectrum using the Eisenstein & Hu (1998) transfer function, corresponds to a one-component fluid approximation. Somogyi & Smith (2009) showed this approximation leads to a biased power spectrum, in particular, for high redshifts and for the baryonic component. However, following their studies, the bias is less than 1% for $z \lesssim 3$. Since this effect is much smaller than the effect we are interested in, we can neglect it. Furthermore, we assume that any modification of the final power spectrum is caused by phenomena which affect the baryonic component in haloes and happen after the halo has collapsed. This implies that haloes collapse in the same way as in a CDM-only Universe. We know this assumption is not completely correct, as van Daalen et al. (2011) have demonstrated that the back reaction of the baryons onto the CDM causes the power spectrum of the CDM component to differ from that of a dark matter only simulation. However, the effect of the back reaction on the total matter power spectrum is smaller than the effect caused by the change of the distribution of baryons.

We start by modifying the density profile to better describe

the distribution of the stars and the gas. Note that the NFW profile with the mass-concentration relations of Duffy et al. (2008) is still used to describe the dark matter distribution. The stellar mass in a halo is much more concentrated than either the gas and dark matter components, and we therefore approximate its distribution by a point mass. To describe the gas component, we use a single β-model, which provides a fair description to X-ray observations in groups and clusters of galaxies (e.g., Cavaliere & Fusco-Femiano 1976; Reiprich & Böhringer 2002; Osmond & Ponmann 2004). The corresponding density profile ρ_{gas}, is given by

$$\rho_{\mathrm{gas}}(r) = \rho_0 \Big[1 + \Big(\frac{r}{\alpha r_{500}} \Big)^2 \Big]^{-3\beta/2}, \qquad (20)$$

where α is the ratio between the characteristic scale of the gas profile (i.e. the core radius) and r_{500}, the radius of a sphere with average density 500 times the critical density. The value for the slope β is usually considered a free parameter in the fit to X-ray data, but we note that for a hydrostatic isothermal sphere its value corresponds to the ratio of the specific energy in galaxies to the specific energy in the hot gas (e.g., King 1972; Jones & Foreman 1984; see also Mulchaey 2000 for a review). Finally, note that although different models have been used in the literature (e.g., Osmond & Ponmann 2004; Arnaud et al. 2010), the differences between these models are too small to be important here.

Our model provides a convenient description of the final mass distribution because even though the parameters depend on the details of the various feedback processes, they can be constrained observationally. The most important observable is the gas fraction as a function of halo mass: the gas has an extended profile and the overall profile depends on the fraction of gas which is left in the halo. This has been measured by McCarthy et al. (2010; 2011) for the OWLS simulations and effectively determines the value of ρ_0 in Eqn. 20. The results are presented in the left panel of Figure 8; it is clear that different feedback models lead to rather different scaling relations.

The values of α and β have been measured from the simulations. We note that these values have a large dispersion and depend on the mass; however, we take here an average value measured over a range of masses $10^{13}\,h^{-1}M_\odot < M_{500} < 10^{15}\,h^{-1}M_\odot$. This corresponds to $\alpha = 0.01$ and $\beta = 0.4$ for the AGN and DBLIMFV1618 models and $\alpha = 0.2$ and $\beta = 0.9$ for the REF model. The power spectrum is mildly sensitive to the choice of the slope β as this slope defines how fast the gas power spectrum declines for large k. The AGN model, for which a large fraction of the gas has been ejected beyond r_{500}, has a power spectrum whose shape is less sensitive to the choice of β.

The right panel shows the relation between M_{500}, the mass of a sphere with average density 500 times the critical density of the universe, and $L_{Ks,\mathrm{BCG}}$, the stellar luminosity of the (central) brightest galaxy of the halo in the $K-$band as predicted by McCarthy et al. (2010) using the metallicity-dependent population synthesis model of Bruzual & Charlot (2003). To constrain the parameters of our extended halo model, we fit a power law to the data in Figure 8 and we find:

$$
\begin{aligned}
f_{\mathrm{gas}}/f_b(r_{500}) &= 0.15 \log_{10}(M_{500}) - 1.49 & \text{REF} \\
f_{\mathrm{gas}}/f_b(r_{500}) &= 0.30 \log_{10}(M_{500}) - 3.40 & \text{DBLIMFV1618} \\
f_{\mathrm{gas}}/f_b(r_{500}) &= 0.40 \log_{10}(M_{500}) - 4.94 & \text{AGN} \\
\log_{10}(L_{Ks,\mathrm{BCG}}) &= 0.62 \log_{10}(M_{500}) + 4.19 & \text{REF} \\
\log_{10}(L_{Ks,\mathrm{BCG}}) &= 0.81 \log_{10}(M_{500}) + 1.39 & \text{DBLIMFV1618} \\
\log_{10}(L_{Ks,\mathrm{BCG}}) &= 0.83 \log_{10}(M_{500}) + 0.23 & \text{AGN}
\end{aligned}
$$

To compute the stellar mass from the stellar luminosity, we measure the average mass-to-light ratio of the BCGs directly from the simulations. We find $M_\star/L_\star = 0.65 M_\odot/K_\odot$ for AGN, $0.32 M_\odot/K_\odot$ for DBLIMV1618, and $0.33 M_\odot/K_\odot$ for REF. We could have measured the stellar mass of the BCG directly from the simulations, but since we want to use quantities which can in principle be observed, we derive the stellar mass using the same procedure that one needs to use for real data.

To determine the fraction of baryons (stars + gas) that remains within r_{500}, we use the scaling relations shown in Figure 8. We then assume that the gas fraction within r_{vir} is the same as within r_{500}, although we note that may not be correct. The resulting halo density profile is the sum of the stellar, gas and dark matter profiles weighted by their respective fractions. We assume that the ejected gas is still associated with the the parent halo and make ad-hoc assumption that the gas is distributed uniformly between $r_{\mathrm{vir}} < r < 2r_{\mathrm{vir}}$. We add this uniform component to the function $y[k, M(\nu)]$ so that the total mass of the halo is unchanged. The density distribution of the gas at large radii can been derived, using X-ray observations, only for bright clusters (Reiprich et al. 2008), and it might be overestimated (Simionescu et al. 2011). Stacked X-ray (e.g., Dai et al. 2010) and SZ observations (e.g., Afshordi et al. 2007; Komatsu et al. 2011) could allow one to obtain a more accurate estimation of the gas distribution even for less massive haloes. We will measure the distribution of this gas using the simulations and evaluate the importance of its modelling in a future work.

Under these assumptions our model has more power than the simulations for high k. This is due to an overestimate of the stellar mass which can be explained as follows. Using the simulations data by McCarthy et al. (2010) we can only establish a relation between M_{500} and $L_{Ks,\mathrm{BCG}}$ for haloes with $M_{500} > 5 \times 10^{12}\,h^{-1}\,M_\odot$. Observationally the relation between the fraction of stars and halo mass is approximately linear down to a certain halo mass; for haloes with mass below a few times $10^{12}\,h^{-1}\,M_\odot$ this relation is poorly constrained. However, observations suggests a stellar fraction for Milky Way size haloes which is about 0.01, suggesting that the stellar-mass to halo-mass relation has to change. This observed relation between luminosity and halo mass agrees well (see e.g. Moster et al. 2010) with models constructed using halo occupation distributions (e.g., Peacock & Smith 2000; Seljak 2000; White 2001; Berlind & Weinberg 2002) and conditional luminosity functions (Yang et al. 2003; van den Bosch et al. 2007; Cacciato et al. 2009), as well as with semi-analytic models (e.g. Croton et al. 2006; Bower et al. 2006). Those approaches all show that there is a characteristic mass $M \approx 10^{12.5}\,h^{-1}\,M_\odot$ for which star formation is particularly efficient, whereas for small masses the fraction of stars in haloes decreases steeply. This should also happen in our simulations although we lack the resolution required to measure the stellar mass-to-light ratio for small haloes. Thus, we just assume that the mass of the stars is $0.01\,M_{500}$ for $M_{500} < 5 \times 10^{12}\,h^{-1}\,M_\odot$ which approximately corresponds to the fraction of stars in a Milky Way size halo. Note that while low-mass haloes do not contribute much at small k, they will dominate the signal if the stellar fraction is too large.

In Figure 9 we compare the ratios of the power spectra measured from the simulations to the ones predicted by the model. Despite its simplicity, the model is able to reproduce the main features of the power spectrum for all scenarios for redshifts to which the weak lensing signal is most sensitive. Although it is a clear improvement over the pure dark matter model, the model is still too simplistic and does not perform equally well at all redshifts and all scales. The accuracy of the toy model can clearly be improved and
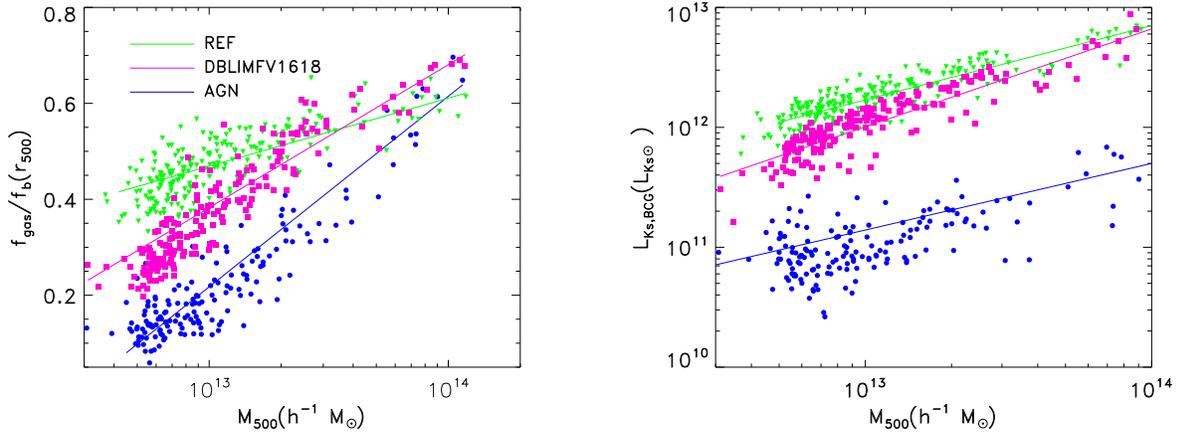
Figure 8. Left panel: relation between M_{500} and gas fraction in haloes for REF, DBLIMFV1618 and AGN. Right panel: relation between M_{500} and the stellar luminosity in the K-band L_{Ks} of the brightest galaxy in the halo. The solid lines represent the best linear fits to the points (see text). The simulation data was taken from McCarthy et al. (2010), who showed that the AGN model agrees with the available observations of groups.
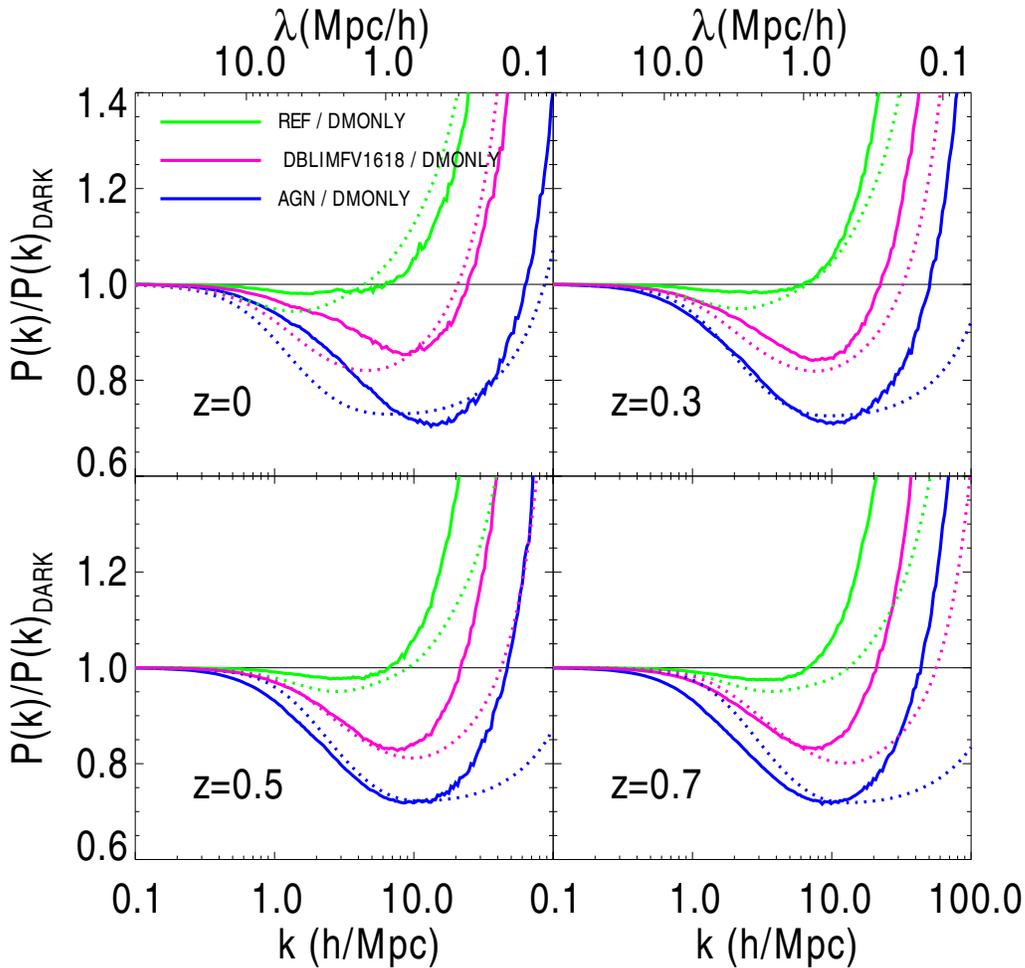

Figure 9. Comparison of the ratio of the power spectra REF/DMONLY, DBLIMFV1618/DMONLY and AGN/DMONLY measured from the simulations (solid lines) and predicted by our simple halo model (dotted lines) which has been tuned to fit the gas and stellar mass fractions predicted in each scenario (see text). The model matches the simulations fairly well for $k < 10\,h\,\mathrm{Mpc}^{-1}$.
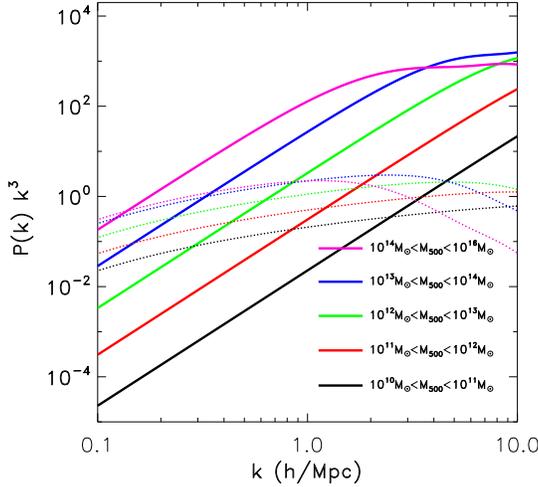
Figure 10. Contribution of haloes of different masses to the one halo-term $P^{\mathrm{P}}(k)$ (solid lines) redshift $z = 0.5$. We show for comparison the halo-halo term $P^{\mathrm{hh}}(k)$ (dotted lines) for the same mass ranges. At scales where the baryonic feedback is important, the dominant contribution is the Poisson contribution of haloes with $M_{500} \gtrsim 10^{13}\,h^{-1}\,M_\odot$.

we will aim to do so in future work. In particular, we will examine requirements on the types of observations that will be needed to constrain the model and the mass and length scales that need to be studied.

Indeed, we remind the reader, that we currently calibrate the model using scaling relations covering a large range of masses; in particular down to low-mass haloes. Figure 10 shows the contributions to the power spectrum from various ranges in halo mass. This demonstrates that haloes with masses $M_{500} > 10^{13}\,h^{-1}\,M_\odot$, i.e. massive galaxies, groups and clusters, contribute most on the scales of interest, but that the properties of halos with masses as low as $10^{12}\,h^{-1}\,M_\odot$ need to be understood as well.

Currently, scaling relations can be measured observationally down to virial masses of a few $10^{13}\,h^{-1}\,M_\odot$, albeit only for biased samples. For those high-mass haloes the parameters of our model can be constrained directly by observations of groups and clusters of galaxies, most notably the gas fraction (e.g., Giodini et al. 2009; Sun et al. 2009). Although studies of ensemble averaged properties can also provide useful constraints (Leauthaud et al. 2010; Rykoff et al. 2008), for masses down to $M_{\mathrm{vir}} \sim 10^{12}\,M_\odot$ observational constraints are expected to remain limited. Furthermore, in our model, we made a rather ad-hoc assumption that the gas that is removed from the central regions is in the outskirts of the haloes. Although this seems plausible (see for example Rasheed et al. 2010) it is not clear how accurately one can observe the distribution of the gas in the outskirts of the haloes. Because of those observational limitations, we expect that an accurate description of the baryonic feedback will have to rely in part on simulations.

Finally, our findings suggests that a model with few parameters, similar to the one we introduced, can capture the main features of the baryonic feedback. Those parameters need to be varied together with the cosmological parameters when one performs a cosmological interpretation. One can use observations and simulations

to derive priors on those parameters and increase the accuracy of the cosmological parameters estimation.

5.3 Improved constraints on cosmological parameters

To examine whether the biases on the cosmological parameters are indeed reduced, we repeat the likelihood analysis described in Section 4, using the improved halo model to compute the lensing signal. The results are presented in Figure 11. For the AGN scenario, where the biases in Ω_{m} and w_0 were $\sim 20\%$ and 40% respectively, the bias is now visible reduced, although it is still larger than the statistical error for a Euclid-like survey.

Despite its simplicity, the model allows for a significant improvement and its accuracy can be further increased. For instance, we did not include any evolution in the scaling relations. We also did not account for the intrinsic dispersion in the model parameters. Furthermore, for the gas that has been ejected beyond r_{500}, we simply assumed an homogeneous distribution, but more work is needed to validate (or improve) this assumption. We will explore various improvements to our model in future work, as they are beyond the scope of this paper.

6   CONSEQUENCES FOR OTHER PARAMETERS

In section 4 we showed that ignoring the effects of baryons on the power spectrum leads to significant biases in the recovered dark energy equation of state w_0, as well as in σ_8 and Ω_{m}. The measurement of these parameters is, however, not the only goal of future cosmic shear studies. In this section we examine the impact of baryon physics on the accuracy of some cosmological parameters for which weak lensing has been suggested to be a useful probe. These are the scale dependence of the spectral index of the primordial power spectrum (section 6.1), the properties of cold dark matter (section 6.2) and the neutrino masses (section 6.3).

6.1   Running of the spectral index

The large-scale structure we observe today is believed to arise from quantum fluctuations that grew to cosmological scales during a period of inflation. Simple models of inflation predict a primordial power spectrum that is nearly scale invariant, $P(k) \propto k^{n_s}$, with scalar spectral index $n_s \approx 1$. In more complicated inflation theories n_s may also depend on k. A general expansion adopted for $n_s(k)$ is (Kosowsky & Turner 1995):

$$n_s(k) = n_s(k_0) + \frac{dn_s}{d\ln k}\ln\left(\frac{k}{k_0}\right) \qquad (21)$$

where $k_0 = 0.015\ \mathrm{Mpc}^{-1}$ is a pivot. A non-zero value for $\alpha_s \equiv dn_s/d\ln k$ results in a running spectral index. Measurements of both n_s and α_s provide direct constraints on the inflationary models, and are thus of great interest. CMB temperature fluctuations as well as CMB polarisation measurements are able to provide constraints on the spectral index. The most recent results from ACT WMAP7 suggest $n_s(k_0)$ to be slightly smaller than unity and $\alpha_s < 0$ (Dunkley et al. 2010).

Weak lensing observations enable us to extend the measurements to smaller scales, thus tightening the constraints on α_s. We are concerned, however, that such a measurement will also be affected by baryon physics, because the suppression in the power spectrum seen for the AGN model could also be achieved by a
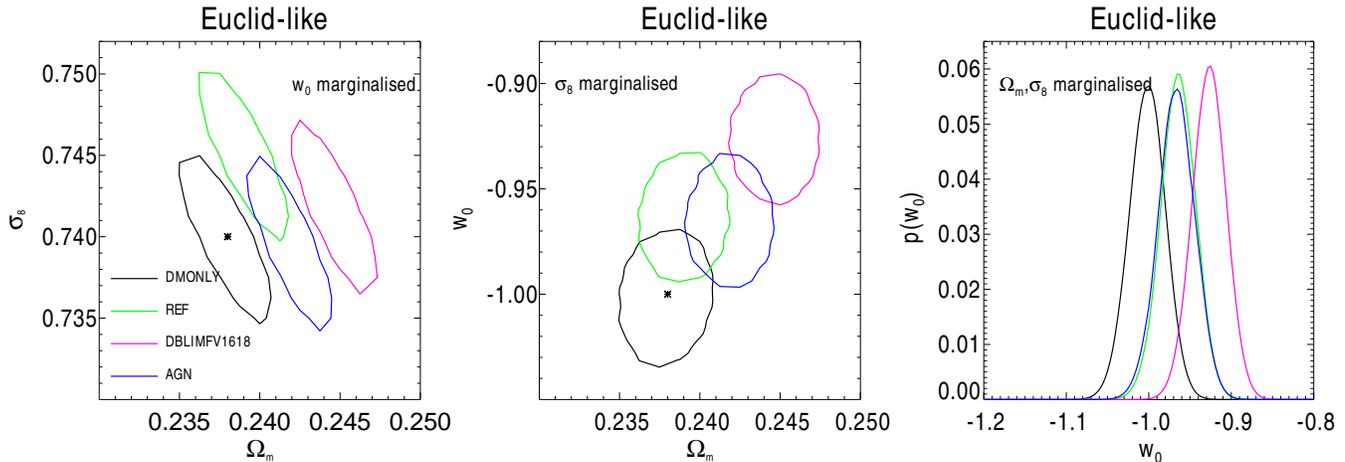
Figure 11. Left panel: joint constraints on Ω_m and σ_8 for a Euclid-like survey, using our improved halo model tuned to fit the gas and stellar mass fractions predicted by each scenario to compute the likelihood. The contours indicate the 68% confidence regions for the various feedback models. Middle panel: joint constraints on Ω_m and w_0. Right panel: posterior probability distribution of w_0 after marginalisation over Ω_m and σ_8. When the improved model is used to compute the lensing signal, the biases in the recovered cosmological parameters are significantly reduced.

more negative value for α_s. This is demonstrated by Figure 12, where we show that it is possible to find dark matter only models (i.e. halofit models) with a running spectral index that match the simulated power spectra for the lowest redshift bin.

We also computed the joint likelihood for $n_s \in [0.90, 1.20]$ and $\alpha_s \in [-0.10, 0.050]$, marginalising over a flat prior $\sigma_8 \in [0.65, 0.83]$ while keeping w_0 and Ω_m fixed. The results are presented in the left panel of Figure 13. As expected, the best-fit value for α_s is biased to a more negative value in the case of the AGN model if the effects of baryons are ignored. Our simple extension of the halo model is able to reduce the bias also for these parameters, as is demonstrated by the right panel in Figure 13.

6.2 Warm dark matter

A number of observations appear to disagree with the outcome of ΛCDM simulations which predict a large amount of structure in galaxy-sized haloes. In particular, the simulations predict a larger number of satellite galaxies for the Milky Way than is observed (the so-called missing satellites problem), although the recent discovery of faint satellites appears to alleviate this problem (see Belokurov et al. 2010). Another longstanding issue concerns the inner slope of the density profile: low surface brightness galaxies show profiles which are not as cuspy as the NFW profile (e.g. Kuzio De Naray et al. 2010; Oh et al. 2010).

The existence of warm dark matter (WDM) can, in principle, solve the problems mentioned above, because the free-streaming of the particles suppresses small-scale fluctuations and leads to haloes with a core. We note, however, that Villaescusa & Dalal (2011) recently showed that WDM haloes cannot form cores that are large enough to match the observations. Recent papers suggest that future weak lensing missions such as Euclid, combined with Planck observations, can constrain the mass of the WDM particles, through the effect they have on the growth of structure (e.g., Marković et al. 2010).

To ensure that structure formation is only altered on small scales, the parameters of WDM models are generally chosen such that that the power spectrum is modified at subgalactic scales
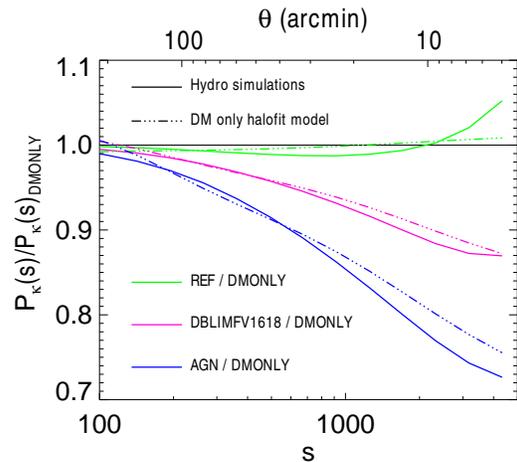

Figure 12. Ratio of the weak lensing power spectra for the lowest redshift tomographic bin, for the REF/DMONLY, DBLIMFV1618/DMONLY and AGN/DMONLY models (solid lines). The dot-dashed lines show the ratio for the dark matter only halofit model that best fits each of the simulations, obtained by varying σ_8, the spectral index $n_s(k_0)$ and the running $\alpha_s = dn_s/d\ln k$. In general it is possible to find a combination of parameters, such that the dark matter only model with a running of the spectral index fits the simulated power spectra reasonably well.

$k_{\rm fs} \simeq 0.1 - 1 h\,{\rm Mpc}^{-1}$, which are also affected by baryon physics. As an example, we consider the case of fully thermalised particles described by Marković et al. (2010). In this case the WDM streams freely shortly before the Universe enters the matter-dominated era. The effect on the power spectrum can be parametrised by (Viel et al. 2005):

$$T(k) = \left(\frac{P_{\rm WDM}(k)}{P_{\rm CDM}(k)}\right)^{1/2} = [1 + (\alpha k)^{(2\mu)}]^{(-5/\mu)}, \quad (22)$$

with $\mu = 1.12$ and where $P_{\rm CDM}(k)$ and $P_{\rm WDM}(k)$ are the CDM

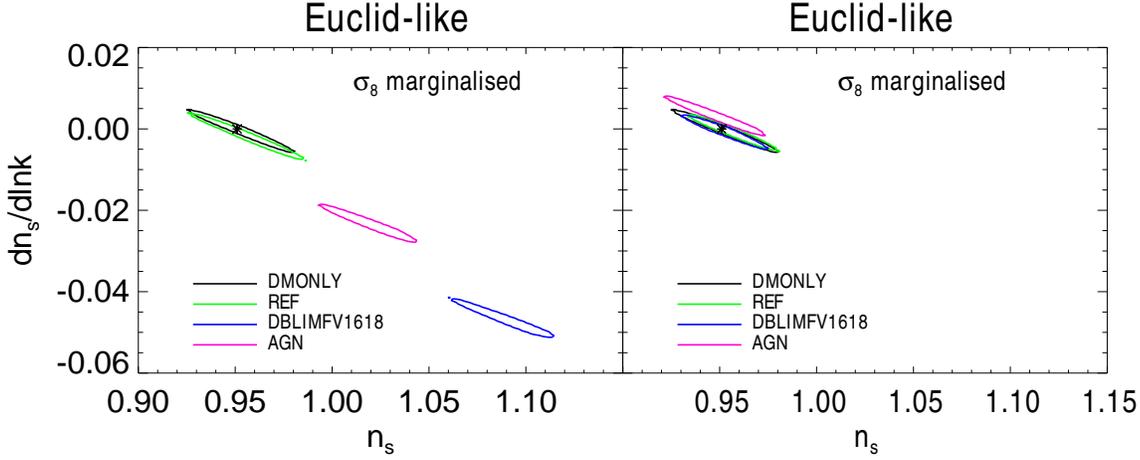**Figure 13.** Left panel: joint constraints on the primordial spectral index $n_s(k_0)$ and running $\alpha_s = dn_s/d\ln k$ after marginalising over σ_8 (while keeping the other parameters fixed) for a Euclid-like survey. The contours indicate the 68% confidence regions for the feedback models that are indicated. Right panel: constraints when we use our extension of the halo model (see Section 5), which was tuned to fit the halo gas fractions and K-band magnitudes predicted by the simulations. The improved halo model partially reduces the level of the bias.

and WDM power spectra, respectively. The value for the break scale α is then given by (Viel et al. 2005):

$$\alpha = 0.049 \left(\frac{m_{\rm WDM}}{\rm keV} \right)^{-1.11} \left(\frac{\Omega_{\rm WDM}}{0.25} \right)^{0.11} \left(\frac{h}{0.7} \right)^{1.22} h^{-1} {\rm Mpc}, \tag{23}$$

where $\Omega_{\rm WDM}$ is the WDM density parameter and $m_{\rm WDM}$ is the WDM particles mass. Observations of the power spectrum of the Lyman-α forest suggest $m_{\rm WDM} > 4{\rm keV}$ (Seljak et al. 2006; Viel et al. 2008; Boyarsky et al. 2009). If we use this limit, we find that for $k = 10\,h\,{\rm Mpc}^{-1}$, which is where the suppression of the total power by baryons is maximal (see Fig. 1), the power spectrum is suppressed by only 5%, which is much smaller than the suppression predicted by the AGN feedback model. The suppression decreases rapidly, being less than a percent for $k = 1\,h\,{\rm Mpc}^{-1}$. One could argue that this result, which has been derived in the linear approximation, is not valid at small scales where the power spectrum is in the non-linear regime. However, Boehm et al. (2005), showed that the non-linear evolution reduces the difference between CDM and WDM models (also see Marković et al. 2011).

We therefore conclude that the effect of WDM on the weak lensing signal is likely to be dwarfed by baryon physics. If we wish to improve upon current constraints on the WDM mass, we would need to be able to compute the effects of baryon physics on the total matter power spectrum to less than a percent for $k \gtrsim 1\,h\,{\rm Mpc}^{-1}$. It is not clear that such accuracy can be achieved.

6.3 Massive neutrinos

Particle physics experiments have conclusively shown that neutrinos have mass and suggest that there are three species. Experiments are also able to measure the differences in the square of the masses, and thus provide a lower bound on the mass of the heaviest neutrino species. The effect of massive neutrinos on the power spectrum is similar to that of warm dark matter. The main difference is that neutrinos are much lighter (i.e, they are considered hot dark mat-

ter). As a consequence, they become non-relativistic in the matter dominated era.

While experiments are designed to measure the mass of the electron neutrino, studies of large-scale structure constrain the total density of neutrinos in the universe. The most recent estimate from WMAP7 is $\sum m_\nu < 1.3\,{\rm eV}$, or $\sum m_\nu < 0.65\,{\rm eV}$ if constraints from baryon acoustic oscillations are included (Komatsu et al. 2011). This yields an upper bound for on the total neutrino density of $\Omega_\nu < 0.02$ for WMAP7, where we used the relation between the neutrino mass and their cosmological density:

$$\Omega_\nu = \frac{\sum m_\nu}{93.8 h^2 {\rm eV}}. \tag{24}$$

As before, massive neutrinos do not modify the power spectrum on scales larger than their free-streaming length, which decreases with time. Therefore there is a $k_{\rm nr}$ below which the power spectrum is not affected (Lesgourgues & Pastor 2006):

$$k_{\rm nr} = 0.018\, \Omega_{\rm m}^{1/2} \left(\frac{m_\nu}{1{\rm eV}} \right)^{1/2}. \tag{25}$$

To compute the effect of neutrinos on the power spectrum, we use the transfer functions given by the Boltzmann code CAMB (Lewis et al. 2000). Figure 14 shows the ratio of power spectra at $z = 0.5$ with neutrino fractions $f_\nu \equiv \Omega_\nu/\Omega_{\rm m} = 0.01$ and $f_\nu = 0.05$. Note that the best-fit WMAP7 cosmology (Komatsu et al. 2011) yields $k_{\rm nr} \lesssim 0.01\,h\,{\rm Mpc}^{-1}$ and $f_\nu < 0.1$.

At intermediate scales our results indicate that neutrinos cause a scale-dependent suppression of the power spectrum. For large k, our calculations, which are based on linear perturbation theory, indicate that the ratio $P_\nu(k)/P_{\rm CDM}(k)$ is (almost) constant with a value $\simeq (1-8f_\nu)$ (Eisenstein & Hu 1998). A concern might be that linear theory does not provide an adequate description. Although the highly non-linear regime has not been studied, the numerical simulations presented in Brandbyge et al. (2008) suggest that our results are sufficiently accurate: $P_\nu(k)/P_{\rm CDM}(k)$ reaches a mini-
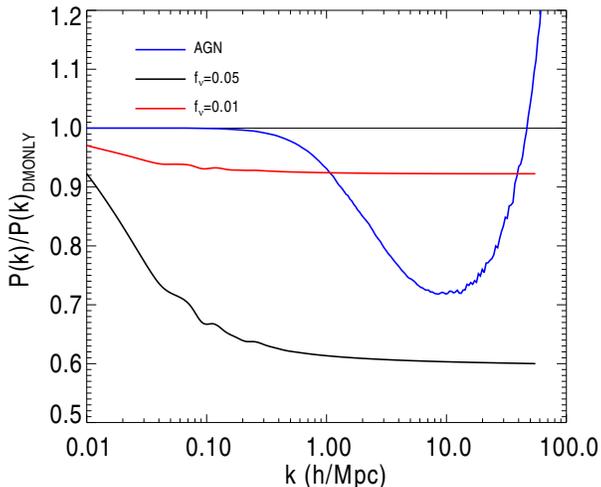
Figure 14. Ratio of the AGN/DMONLY power spectra (blue line), and dark matter power spectra with $f_\nu \equiv \Omega_\nu/\Omega_\mathrm{m} = 0.01$ and 0.05, which correspond to neutrino masses of $\sum m_\nu \sim 6.0$ and $\sum m_\nu \sim 1.2$ eV, respectively. The effect of massive neutrinos on the power spectrum is quite different from that of baryon physics, even if neutrinos are light.

mum value of $\sim (1-10f_\nu)$ and slightly increases again for smaller k. The results presented in Figure 14 indicate that for $f_\nu \sim 0.05$ (or a mass of $\sum m_\nu \sim 6.0$ eV) the suppression of power by massive neutrinos dominates over the baryon physics. In the case of light neutrinos ($\sum m_\nu \sim 1.2$ eV or $f_\nu = 0.01$), baryon physics dominates for $k > 1\,h\,\mathrm{Mpc}^{-1}$, but the neutrinos cause a significant suppression of power on intermediate scales. Thus, it seems likely that one would be able to get useful constraints using only large-scale measurements.

7 CONCLUSIONS

Weak gravitational lensing by large-scale structure is a powerful technique to study the properties of dark matter and dark energy. However, the interpretation of the signal requires comparison to a predicted matter power spectrum. To date, such cosmic shear measurements have used predictions based on numerical simulations of cold dark matter. As the precision of future projects improves, the effects of baryon physics need to be quantified. Recently, van Daalen et al. (2011) have shown that the impact of baryonic feedback is significant and demonstrated that the precision with which one is able to predict the matter power spectrum from simulations depends on how well one understands and models mechanisms such as radiative cooling, star formation, metal enrichment, supernovae and AGN feedback. In particular, they have shown that baryon physics modifies the matter power spectrum to a level which is higher than the accuracy required for future weak lensing experiments, which require predictions for the amplitude of the power spectrum with an accuracy of a few percent for a large range of scales.

In this paper we made a first attempt to quantify the effect of baryon physics on the cosmic shear signal, using a subset of the cosmological hydrodynamic simulations that were carried out as part of the OWLS project (Schaye et al. 2010) and for which the matter power spectra have been measured by van Daalen et al (2011).

We find that if weak lensing measurements are interpreted using a power spectrum that ignores the effects of baryon physics, the resulting cosmological parameter estimates are biased. The bias depends on the feedback model, but is as large as $\sim 40\%$ for the dark energy equation of state w_0 for the AGN scenario, which we consider our most realistic model as it reproduced the observed X-ray and optical properties of groups of galaxies (McCarthy et al. 2010). The biases dominate over the statistical errors for Euclid, a proposed space mission that aims to measure w_0 with a precision of a few percent.

The reason for the large bias is the fact that efficient feedback modifies the power spectrum out to several megaparsecs, contrary to the commonly held belief that only very small scales are affected, as is the case in previous models that suffered from the "overcooling" problem. To reduce the bias to acceptable levels, one would need to discard scales smaller than ~ 40 arcminutes from the weak lensing analysis in the case of Euclid, at the expense of a factor three increase in the statistical error.

Such a large reduction in sensitivity to the dark energy properties is not desirable. Instead, we explored an approach to reduce the bias, based on a simple extension of the halo model. We treat the dark matter, gas and stars as separate components, assigning suitable profiles to each. The baryonic mass assigned to each component is determined using scaling relations between the halo mass and the gas fraction and stellar mass. For each scenario the model parameters were constrained by fitting the simulated gas fraction and stellar masses of groups and clusters at redshift $z = 0$. We also made the ad-hoc assumption that the ejected gas is distributed uniformly between the virial radius and $2r_{\mathrm{vir}}$. Further work is needed to improve upon this assumption.

Although several improvements should be made (an issue that we will explore in future work), the simple model presented here is able to describe the OWLS power spectra fairly well for $k < 10\,h\,\mathrm{Mpc}^{-1}$. Particularly encouraging is the reduction in the bias in w_0 and the other cosmological parameters.

The usefulness of our model hinges partly on our ability to calibrate the model though observations of the distribution of gas and stars in halos with masses as low as $10^{12}\,h^{-1}\,M_\odot$, which may be too low for X-ray and SZ observations. Moreover, in order to achieve the precision required for future weak lensing experiments, one would need to know the distribution of the gas in the peripheral regions of haloes. This suggests that improvements require a 'hybrid' approach, relying on a combination of deeper observations and better simulations. For instance, dedicated X-ray and SZ studies can help calibrate the model parameters, but they also provide constraints on the accuracy of the hydrodynamic simulations.

Finally, we also examined the effects of baryon physics on other applications of weak lensing. For Euclid, constraints on the parameters of the primordial power spectrum predicted by theories of inflation are also significantly biased. The measurement of the neutrino mass is also affected (in particular if the mass is small), but the bias should be small if only scales larger than ~ 10 Mpc are considered. Improved weak lensing constraints on the properties of warm dark matter are unlikely, because current constraints lead to changes in the power spectrum that are much smaller than those introduced by baryon physics.

REFERENCES

Albrecht A., et al., 2006, APS meeting abstract, APR, G1002, arXiv:astro-ph/0609591

Allen S. W., Rapetti D. A., Schmidt R. W., Ebeling H., Morris R. G., Fabian A. C., 2008, MNRAS, 383, 879

Amanullah R., et al., 2010, ApJ, 716, 712

Arnaud M., Pratt G. W., Piffaretti R., Böringer H., Croston J. H., Pointecouteau E., 2010, A&A, 517, 92

Afshordi N., Lin Y.-T., Nagai D., Sanderson A. J. R., 2007, MNRAS, 378, 293

Bartelmann M., Schneider P., 2001, Physics Reports, 340, 291, arXiv:astro-ph/9912508

Bartko H., et al., 2010, ApJ, 708, 834

Baugh C. M., Lacey C. G., Frenk C. S., Granato G. L., Silva L., Bressan A., Benson A. J., Cole S., 2005, MNRAS, 356, 1191

Belokurov V. et al, 2010, ApJ, 712, L103

Benjamin J., et al. , 2007, MNRAS, 381, 702

Berlind A. A., Weinberg D. H., 2002, ApJ, 575, 587

Bernstein G. M., 2009, ApJ, 695, 652

Boehm C., Mathis H., Devriendt J., Silk J., 2005, MNRAS, 360, 282

Booth C., Schaye J., 2009, MNRAS, 358, 53

Bower R. G., Benson A. J., Malbon R., Helly J. C., Frenk C. S., Baugh C. M., Cole S., Lacey C. G., 2006, MNRAS, 370, 645

Boyarsky A., Lesgourgues J., Ruchayskiy O., Viel M., 2009, JCAP, 05, 012

Brandbyge J., Hannestad S., Haugbølle T., Thomsen B., 2008, JCAP, 08, 020B

Bruzual G., Charlot S., 2003, MNRAS, 344, 1000

Bryan G. L., Norman M. L., 1998, ApJ, 495, 80

Cacciato M., van den Bosch F. C., More S., Li R., Mo H. J., Yang X., 2009, MNRAS, 394, 929

Casarini L., Macciò A. V., Bonometto S. A., Stinson G. S., 2011, MNRAS, 412, 911

Cavaliere A., Fusco-Femiano R.,1976, A&A, 49, 137

Chabrier G., 2003, PASP, 115, 763

Croton D. J., et al., 2006, MNRAS, 365, 11

Dabringhausen J., Kroupa P., Baumgardt H., 2009, MNRAS, 394, 1529

Dai X., Bregman J. N., Kochanek C. S., Rasia E., 2010, ApJ, 719, 119

Dalla Vecchia C., Schaye J., 2008, MNRAS, 383, 1210

Duffy A. R., Schaye J., Kay S. T., Dalla Vecchia C., 2008, MNRAS, 390, 64

Duffy A. R., Schaye J., Kay S. T., Dalla Vecchia C., Battye R. A., Booth C. M., 2010, MNRAS, 405, 2161

Dunkley J., et al., 2010, ApJ submitted, ArXiv:astro-ph/1009.0866

Eisenstein D. J., Hu W., 1998, ApJ, 496, 605

Eisenstein D. J., et al. 2005, ApJ, 633, 560

Fu L., et al., 2008, A&A, 479, 9F

Giodini S., et al., 2009, ApJ, 703, 982

Guillet T., Tessyer R., Colombi S., 2010, MNRAS, 405, 525

Heitmann K., White M., Wagner C., Habib S., Higdon D., 2010, ApJ, 715, 104

Hoekstra H., Mellier Y., van Waerbeke L., Semboloni E., Fu L., Hudson M. J., Parker L., Tereno I., Benabed K., 2006, ApJ, 647, 116

Hoekstra H., Jain B., 2008, Annual Review of Nuclear and Particle Systems, 58, 99, arXiv:astro-ph/0805.0139

Hu W., 1999, ApJ, 522, L21

Hu W., 2002, Phys Rev D, 66, 8

Jing Y. P., Zhang P., Lin W. P., Gao L., Springel V., 2006, ApJ, 640, 119

Jones C., Foreman W., 1984, ApJ, 276, 38

Kaiser N., 1998, ApJ, 498, 26

King I. R., 1972, ApJ, 174, L123

Kitching T. D., Taylor A. N., 2010, MNRAS, submitted, arXiv:astro-ph/1012.3479

Klessen R., Spaans M., Jappsen A. K., 2007, MNRAS, 374, L29

Komatsu E., et al., 2011, ApJS, 192, 18

Kosowsky A., Turner M. S., 1995, Phys. Rev. D, 52, 1739

Kuzio De Naray R., Martinez G. D., Bullock J. S., Kaplinghat M., 2010, ApJ, 710, L161

Laurejis R., et al. (Euclid Science Study Team), 2009, Euclid Assessment Study Report for the ESA Cosmic Visions, arXiv:astro-ph/0912.0914

Leauthaud A., et al., 2010, ApJ, 709, 97

Lesgourgues J., Pastor S., 2006, PhR, 429, 307

Levine R., Gnedin N. Y., 2006, ApJ, 649, L57

Lewis A., Challinor A., Lasenby A., 2000, ApJ, 538, 473

Mandelbaum R., Tasitsiomi A., Seljak U., Kravstov A., Wechsler R. H., 2005, MNRAS, 362, 1451

Maness H., et al., 2007, ApJ, 618, 569

Markovič K., Bridle S., Slosar A., Weller J., 2011, JCAP, 1, 22

Massey R., et al., 2007, MNRAS, 376, 13

McCarthy I. G., Schaye J., Ponmann T. J., Bower R. G., Booth C. M., Dalla Vecchia C., Crain R. A., Springel V., Theuns T., Wiersma R. P. C., 2010, MNRAS, 406, 882

McCarthy I. G., Schaye J., Bower R. G., Ponman T. J., Booth C. M., Dalla Vecchia C., Springel V., 2011, MNRAS, 412, 1965

Moster B. P., Sommerville R. S., Maulbetsch C., van dan Bosch F. C., Macciò A. V., Naab T., Oser L., 2010, ApJ, 710, 903

Mulchaey J. S., 2000, Annual Review of Astronomy & Astrophysics, 38, 289, arXiv:astro-ph/0009379

Munshi D., Valageas P., van Waerbeke L., Heavens A., 2008, Physics Reports, 462, 67, arXiv:astro-ph/0612667

Navarro J. F., Frenk C. S., White S. D. .M, 1995, MNRAS, 275, 720

Oh S.-H., Blok W. J. G., Brinks E., Walter F., Kennicutt R. J., 2010, AJ, 141, 193

Osmond J. P. F., Ponmann T. J., 2004, MNRAS, 350, 1511

Padoan P., Nordlund A., Jones B. J. T., 1997, MNRAS, 288, 145

Peacock J. A., Dodds S. J., 1996, MNRAS, 280, L19

Peacock J. A., Smith R. E., 2000, MNRAS, 318, 1144

Percival W. J., et al. 2010, MNRAS, 401, 2148

Perlmutter S., et al., 1999, ApJ, 517, 565

Pielorz J., Rödiger J., Tereno I., Schneider P., 2010, A&A, 514, 79

Rasheed B., Bahcall N., Bode P., 2010, PNAS submitted, arXiv:astro-ph/1007.1980

Refregier A., et al., 2010, arXiv:astro-ph/1001.0061

Reiprich. T., Böringer H., 2002, A&A, 567, 716

Reiprich. T., Hudson D. S., Zhang Y.-Y., Sato K., Ishisaki Y., Hoshino A., Ohashi T., Ota N., Fujita Y., 2008, A&A, 501, 899

Riess A. G., Strolger L. G., Casertano S., Ferguson H. C., Mobasher B., Gold B., Challis P. J., Filippenko A. V., Jah S., Li W., Tonry J., Foley R., Kirshner R. P., Dickinson M., MacDonald E., Eisenstein D., Livio M., Younger J., Xu C., Dahlén T., Stern D., 2007, ApJ, 659, 98

Rudd D. H., Zenter A. R., Kravtsov A. V., 2008, ApJ, 672, 19

Rykoff E. S., et al., 2008, MNRAS, 387, L28

Schaye J., Dalla Vecchia C., 2008, MNRAS, 383, 1210

Schaye J., Dalla Vecchia C., Booth C., Wiersma R. P. C., Theuns T., Haas M. R., Bertone S., Duffy A. R., McCarthy I. G., van de Voort F., 2010, MNRAS, 402, 1536

Schneider P., van Waerbeke L., Jain B., Kruse G., 1998, MNRAS, 296, 873

Schrabback T., et al., 2010, A&A, 516, 63

Seljak U., 2000, MNRAS, 318, 203

Seljak U., Makarov A., McDonald P., Hy T., 2006, Phys. Rev. Letters, 97, 19

Semboloni E., van Waerbeke L., Heymans C., Hamana T., Colombi S., White M., Mellier Y., 2007, MNRAS, 375, 6

Simionescu A., et al., 2011, Science, 331, 1576

Sheth R. K., Tormen G., 1999, MNRAS, 308, 119

Smith R. E., et al., 2003, MNRAS, 341, 1311

Somogyi G., Smith R. E., 2010, Phys. Rev. D, 81, 023524

Spergel D., et al., 2007, ApJS, 170, 377

Springel V., 2005, MNRAS, 364, 1105

Sun M., Voit G. M., Donahue M., Jones C., Forman W., Vikhlinin A., 2009, ApJ, 693, 1142

Takada M., Jain B., 2004, MNRAS, 348, 897

Takada M., Jain B., 2009, MNRAS, 395, 2065

van Daalen M. P., Schaye J., Booth C. M., Dalla Vecchia C., 2011, MNRAS, 415, 3649

van den Bosch F. C., Yang X., Mo H. J., Weinmann S., Macciò A., More S., Cacciato M., Skibba R., Kang X., 2007, MNRAS, 376, 841

Viel M., Lesgourgues J., Haehnelt M. G., Matarrese S., Riotto A., 2005, Phys Rev D, 71, 6

Viel M., Becker G. D., Bolton J. S., Haehnelt M. G., Rauch M., Sargent W. L. W., 2008, Phys Rev Letters, 100, 4

Villaescusa-Navarro F., Dalal N., 2011, JCAP, 03, 024

Uzan J. P., 2007, Gen. Rel. Grav., 39, 307

Weidner C., Kroupa P., Pflamm-Altenburg J., 2010, MNRAS, 412, 979

White M., 2001, MNRAS, 321, 1

Wiersma R. P. C., Schaye J., Smith B. D., 2009, MNRAS, 393, 99

Wiersma R. P. C., Schaye J., Theuns T., Dalla Vecchia C.,Tornatore L., 2009, MNRAS, 399, 574

Yang X. Mo H. J., van den Bosch F. C., 2003, MNRAS, 339, 1057

Zentner A. R., Rudd D. H., Hu W., 2008, Phys. Rev. D, 77, 043507